From structure to dynamics: frequency tuning in the p53-Mdm2 network I. Logical approach

Wassim Abou-Jaoudé, Djomangan A. Ouattara, Marcelle Kaufman

www.elsevier.com/locate/yjtbi

From structure to dynamics: frequency tuning in the p53-Mdm2 network I. Logical approach

Wassim Abou-Jaoudé, Djomangan A. Ouattara, Marcelle Kaufman

PII: S0022-5193(09)00068-X
DOI: doi:10.1016/j.jtbi.2009.02.005
Reference: YJTBI5462

To appear in: *Journal of Theoretical Biology*

Received date: 10 September 2008
Revised date: 19 January 2009
Accepted date: 11 February 2009

Cite this article as: Wassim Abou-Jaoudé, Djomangan A. Ouattara and Marcelle Kaufman, From structure to dynamics: frequency tuning in the p53-Mdm2 network I. Logical approach, *Journal of Theoretical Biology* (2009), doi:10.1016/j.jtbi.2009.02.005

From structure to dynamics: Frequency tuning in the p53-Mdm2 network
I. Logical approach

Wassim Abou-Jaoudé, Djomangan A. Ouattara, Marcelle Kaufman*
Université Libre de Bruxelles (U.L.B.), Faculté des Sciences, Unit of Theoretical and Computational Biology, Campus Plaine C.P. 231, B-1050 Brussels, Belgium.

***Corresponding author:**
Marcelle Kaufman
Université Libre de Bruxelles (U.L.B.), Faculté des Sciences,
Unit of Theoretical and Computational Biology,
Campus Plaine C.P. 231, B-1050 Brussels, Belgium
E-mail: Marcelle.Kaufman@ulb.ac.be
Tel.: +32 2 650 57 73
Fax: +32 2 650 57 67

Abstract

We investigate the dynamical properties of a simple four-variable model describing the interactions between the tumor suppressor protein p53, its main negative regulator Mdm2 and DNA damage, a model inspired by the work of Ciliberto et al. (2005). Its core consists of an antagonist circuit between p53 and nuclear Mdm2 embedded in a 3-element negative circuit involving p53, cytoplasmic and nuclear Mdm2. A major concern has been to develop an integrated approach in which various types of descriptions complement each other. Here we present the logical analysis of our network and briefly discuss the corresponding differential model. Introducing the new notion of "logical bifurcation diagrams", we show that the essential qualitative dynamical properties of our network can be summarized by a small number of bifurcation scenarios, which can be understood in terms of the balance between the positive and negative circuits of the core network. The model displays a wide variety of behaviours depending on the level of damage, the efficiency of damage repair and, importantly, the DNA-binding affinity and transcriptional activity of p53, which are both stress- and cell-type specific. Our results qualitatively account for several experimental observations such as p53 pulses after irradiation, failure to respond to irradiation, shifts in the frequency of the oscillations, or rapid dampening of the oscillations in a cell population. They also suggest a great variability of behaviour from cell to cell and between different cell-types on the basis of different post-translational modifications and transactivation properties of p53. Finally, our differential analysis provides an interpretation of the high and low frequency oscillations observed by Geva-Zatorsky et al. (2006) depending on the irradiation dose. A more detailed analysis of our differential model as well as its stochastic analysis will be developed in a next paper.

Keywords: p53, DNA-damage response, feedback loops, post-translational modifications, network dynamics, mathematical modelling.

1. Introduction

Protein p53 is a transcriptional regulator of a large number of genes involved notably in growth arrest, DNA repair, apoptosis and cellular senescence (Gatz and Wiesmüller, 2006; Oren, 2003; Vogelstein et al., 2000). It therefore plays an essential role in the control of the proliferation of abnormal cells. The level of this key tumour suppressor protein is tightly regulated by the ubiquitin ligase Mdm2 through a negative feedback circuit. This negative circuit prevents the permanent presence of high levels of p53 that would be lethal for the cells. Normally, the level of p53 remains low. It becomes elevated only when cells are stressed or damaged, for example by ionizing radiations, aberrant growth signals or drugs. In particular, the DNA damage resulting from ionizing radiations leads to an increase in the level of active p53, which in turn activates the damage repair process or the synthesis of pro-apoptotic proteins, thereby preventing the proliferation of genetically unstable cells.

The importance of the regulation of p53 for ensuring an appropriate response to various genotoxic and cytotoxic stresses has led to an impressive amount of experimental investigations, some of which deal with the kinetics of the p53 response to DNA damage. In particular, experimental studies on irradiated cells in culture have shown the occurrence of damped oscillations of p53 at the level of cell populations (Bar-Or et al., 2000) and repeated p53 pulses in single cells (Lahav et al., 2004). In these first experiments on single cells, performed with a short time scale, the pulse amplitudes and interpulse intervals were initially reported to remain almost constant, with an average number of peaks increasing with irradiation intensity. Damped p53 oscillations following irradiation were also observed *in vivo* in an Mdm2-luciferase transgenic mouse model (Hamstra et al., 2006), confirming the pulsatile behaviour observed *in vitro*. In more recent experiments, over longer times of observation, Geva-Zatorsky et al. (2006) highlighted several new characteristics of the p53 oscillatory response to DNA damage. They reported, in particular, that under identical conditions, individual cells show a great variability in response to radiation damage, with some cells showing undamped oscillations for at least 3 days while others do not respond or show irregular fluctuations. The oscillations have a regular periodicity and peak width but highly variable amplitudes. A Fourier analysis of the oscillations revealed that the oscillation period decreases with increasing irradiation intensity, with a typical cycling time of about 10 hrs at low irradiation doses and about 6 hrs at high irradiation doses.

The same group also observed that, in some cells, the oscillations stopped or changed frequency after one or two days. On the other hand, in an experimental study of the kinetics of the p53-Mdm2 response for different production rates of p53 and Mdm2, Hu et al. (2007) reported that oscillations only occurred when the basal levels of p53 and Mdm2 are within an optimal range.

Several theoretical models have been proposed to account for the oscillatory behaviour observed experimentally after exposure to stress, either at the level of cell populations (Bar-Or et al., 2000; Ma et al., 2005; Monk, 2003; Ogunnaike, 2006; Tiana et al, 2002) or at the level of individual cells (Bottani and Grammaticos, 2007; Chickarmane et al., 2005; Ciliberto et al., 2005; Geva-Zatorsky et al., 2007; Ma et al., 2005; Puszyński et al., 2008; Wagner et al., 2005; Zhang et al., 2007). They all rely on the well-established negative feedback circuit between p53 and its main antagonist Mdm2, but differ by how this negative circuit is assumed to generate robust large amplitude pulses in the presence of DNA damage. Two broad classes of models can be distinguished. In a first class of models, the occurrence of a robust oscillatory response to stress is ensured by the presence of a sufficiently long time delay between the accumulation of active p53 and the p53-dependent activation of the *Mdm2* gene. In the framework of this type of models, based on ordinary differential equations involving several intermediate steps (Bar-Or et al., 2000; Chickarmane et al., 2005; Puszyński et al., 2008) or on time delayed differential equations (Bottani and Grammaticos, 2007; Ma et al., 2005; Monk, 2003; Ramalingam, 2007; Tiana et al., 2002; Wagner et al., 2005), the transition between a stable steady state with low p53 level and stable oscillations of p53 takes place through a Hopf bifurcation and the onset of large amplitude oscillations requires considering highly nonlinear, switch like, DNA-damage response functions (Chickarmane et al., 2005; Ma et al., 2005). More recently, Batchelor et al. (2008) proposed that repeated, large amplitude p53 pulses would result from the interplay between the basic negative p53-Mdm2 feedback loop and a second negative loop involving upstream regulators of p53. In a second class of models, first developed by Ciliberto et al. (2005), the negative p53-Mdm2 feedback circuit is combined with positive feedback circuits, which upon damage induction leads to an abrupt transition from the homeostatic rest state to oscillations of large and roughly constant amplitude (Zhang et al., 2007). In particular, in the differential model of Ciliberto et al. (2005), as well as in the recent stochastic model of Puszyński et al.

(2008), p53 indirectly amplifies its own level via a PTEN-dependent inhibitory effect on the nuclear entry of Mdm2.

The possible implications of p53 oscillations for the regulation of p53-induced apoptosis still remain an open question and are the subject of a number of recent theoretical analyses (Bose and Ghosh, 2007; Puszyński et al., 2008; Zhang et al., 2007).

In our work, we focused on a simple four-variable model describing the interactions between protein p53, its negative regulator Mdm2 and DNA damage, a model inspired by the work of Ciliberto et al. (2005). Its core consists of an antagonist circuit between p53 and nuclear Mdm2 embedded in a 3-element negative circuit involving p53, cytoplasmic and nuclear Mdm2. To study the dynamics of this network upon damage induction, we combined a multilevel logical modelling method with differential and stochastic approaches. The logical description provided a powerful way of grasping the main qualitative dynamical properties to be expected for our network, without having to specify the details of the molecular interactions or to introduce precise kinetic parameter values. The differential approach allowed us relaxing the high nonlinearity intrinsic to the discrete description and provided more quantitative information on the evolution dynamics. Stochastic simulations further enabled us to account for the effect of molecular fluctuations due to a small number of molecules.

This paper deals with the logical analysis of our model and briefly presents some results of the differential analysis. It introduces new developments of the logical method initially formulated by Thomas (Thomas, 1973; Thomas, 1991; Thomas and D'Ari, 1990), namely (1) the concept of "logical bifurcation diagrams", which enables a systematic characterization of all the asymptotic behaviour compatible with a given set of interactions, and (2) the use of on/off time delays that vary in the course of the evolution of the system for describing the dynamics. Using these tools, we show that the main qualitative dynamical properties of our network can be summarized in terms of a small number of logical bifurcation diagrams that correspond to different bifurcation scenarios and rely on the balance between the positive and negative circuits involving p53. The same simple model displays a wide variety of behaviours depending on the level of damage, the efficiency of damage repair and, importantly, the DNA-binding affinity and transcriptional activity of p53, which are both stress- and cell-type specific (Feng et al., 2007; Mayo, et al., 2005; Singh et al., 2002).

Our results reproduce several qualitative features of the experimental observations for single cells and cell populations and, in particular, the high and low frequency oscillations observed by Geva-Zatorsky et al. (2006) depending on the irradiation dose. They also suggest a high variability of behaviour from cell to cell and between different cell types characterized, for example, by different post-translational modifications and transactivation properties of p53.

This study further emphasizes the link between the structure of a regulatory network and its main dynamical properties as well as the complementarities between the logical and differential approaches. A detailed analysis of our differential model and its stochastic analysis are developed in a next paper.

The outline of the paper is as follows. After a brief presentation of the biological bases of our model in the next section, we summarize the main principles of our logical formalism in Section 3. Section 4 deals with the logical bifurcation analysis of the core of our network and gives some illustrations of the dynamics of single cells upon damage induction as a function of the level of damage and the rate of damage repair. Stochastic logical simulations account for damped oscillations at the level of cell populations. In Section 5, we introduce the differential counterpart of our logical model. We show that the essential results of our logical analysis are preserved for more realistic nonlinearities and parameter values and propose a mechanism for the adjustment of the oscillation frequency as a function of the damage level and repair efficiency.

2. The model

In the present study, we investigate the dynamical properties of a four-variable model derived from the work of Ciliberto et al. (2005). This model describes the interactions between protein p53, the ubiquitin ligase Mdm2 and DNA damage, and is based on well-documented biological data. For short:

- The nuclear component of Mdm2 down regulates the level of active p53. This occurs both by accelerating p53 degradation through ubiquitination (Brooks and Gu, 2006; Haupt et al., 1997; Honda and Yasuda, 2000) and by blockage of the transcriptional activity of p53 (Chen et al., 1995; Coutts et al., 2007; Momand et al., 1992; Oliner et al., 1993; Xirodimas et al., 2004).
- Protein p53 plays a dual role. On the one hand, it positively regulates gene *Mdm2* thereby up-regulating the level of cytoplasmic Mdm2 (Barak et al., 1993;

Freedman et al., 1999) and, on the other hand, it down-regulates the level of nuclear Mdm2 by inhibiting Mdm2 nuclear translocation through inactivation of the kinase Akt (Gottlieb et al., 2002; Mayo and Donner, 2002; Stambolic et al., 2001). It is to be noted that Akt inactivation involves several, PTEN-dependent and independent pathways, whose relative contributions may vary among different cell types as well as between normal and malignant cells, and depend on the stress intensity (Feng et al., 2007; Mayo et al., 2005; Oren et al., 2002; Singh et al., 2002).

- DNA damage is induced by exposure to stress and has a negative influence on the level of nuclear Mdm2, by accelerating its degradation through ATM-mediated phosphorylation and auto-ubiquitination (Stommel and Wahl, 2004; Stommel and Wahl, 2005). This damage-induced Mdm2 destabilization enables p53 to accumulate and remain active.
- High levels of p53 promote damage repair by inducing the synthesis of DNA repair proteins (Adimoolam and Ford, 2003; Gatz and Wiesmüller, 2006; Lozano and Elledge, 2000; Offer et al., 1999).

To define the logical regulatory network that describes the essential features of the system we reformulate the interactions described above as follows: (1) Nuclear Mdm2 down regulates the level of p53 and is itself up regulated by cytoplasmic Mdm2 (nuclear entry); (2) p53 exerts a positive control on the level of cytoplasmic Mdm2 (transcriptional activation) and a negative control on the level of nuclear Mdm2 (blockage of Mdm2 nuclear entry); (3) DNA damage exerts a negative control on the level of nuclear Mdm2 and is itself down regulated by p53. The influence diagram shown in Figure 1 summarizes these interactions.

3. Asynchronous logical approach

We use here the generalized logical description developed by Thomas and colleagues (Snoussi, 1989; Snoussi and Thomas, 1993; Thomas et al., 1995; Thomas and Kaufman, 2001a). The main features of this approach are summarized below. Further extensions of the method that allow handling large and complex systems can be found in Fauré et al. (2006) and Gonzalez et al. (2006).

(1) To each component of a network one associates a discrete variable that represents its level of concentration. These variables take a limited number of integer values, 0 and

1 in the simplest case, indicating that the concentration of a product is below or above a given activity threshold. Threshold values that separate the integer values can also be considered, yielding the scale (0, s_1, 1, s_2, 2, …). The rationale behind the use of multi-valued variables is not to approximate as closely as possible a continuous description, but rather to account for the fact that when a variable influences the level of several targets (including possibly its own level), different concentration thresholds may have to be considered for the different interactions. Note that what is important in the logical description is the order of the thresholds associated with a variable, not their precise value (see, for example, Figure 2).

(2) A set of discrete parameters K, called logical parameters, qualify the weight of each interaction or combination of interactions that act on a variable. These parameters determine, at any time, the logical level towards which the corresponding variable tends to evolve as a function of the present state of the system. The evolution of a component will depend not only on its rate of production, but also on its rate of degradation. Accordingly, the logical parameters correspond to the ratio of the rates of production and decay of a variable and take the value *m* when this ratio exceeds the *m*th threshold of the variable. For each variable x, we shall denote by $K_{x,\{y\}}$ the logical parameter defining the level that x tends to reach when y is present above its relevant threshold of activity. As shown in Appendix A.1, if two logical parameters, say K_x and $K_{x,\{y\}}$, are equal, it does not mean that variable y has no effect on variable x, but rather that its effect is weak.

(3) A state of the network is described by a vector containing the current values of each variable. Given a state of the system, one can identify the set of interactions that are operating upon each component and determine the relevant logical parameter for each variable. If the value of this parameter is higher or lower than the value of the corresponding variable, there is a call for the variable to increase or decrease, respectively, its value. Each change corresponds to a transition to the neighboring integer level (i.e., an increase or decrease by 1) and will effectively be accomplished after a characteristic time delay, unless a counter order is received before the delay has elapsed.

(4) Since a state vector and its corresponding logical parameter vector may differ at the level of more than one variable, a state may have more than one possible next state, depending on which variable is updated first. On the basis of a fully asynchronous

approach, this leads to a transition graph that gives all possible sequences of states of the system, starting from any initial state. Which pathway will actually be followed depends on the values of the time delays associated with different processes and variables, more precisely, on inequalities involving linear combinations of these time delays (Thomas, 1978). Thus, the values of the logical parameters determine all the possible trajectories while the time delays determine which of these trajectories will effectively be followed. When each variable and the corresponding logical parameter have the same value, there is no updating call and one deals with a stable steady state.

(5) An interesting aspect of the generalized logical method is that it allows analysing the dynamic properties of a network in terms of the "functionality" of its constitutive feedback circuits. Clearly, the effect of a circuit does not only depend on the mere existence of the relevant interactions, but also on their relative strength. When appropriate parametric conditions are fulfilled, a circuit will be functional: it will generate multistationarity or multistability if it is a positive circuit, homeostasis, with or without oscillations, if it is a negative circuit (Naldi et al., 2007; Remy et al., 2008; Richard and Comet, 2007; Snoussi, 1993). The notion of circuit functionality is illustrated on a simple example in Appendix A.2.

In addition to these classical features of the generalized logical description, we will introduce here the new notions of logical bifurcation diagrams and time delays that vary in the course of the evolution of the system.

4. Logical modelling of single cell and cell population dynamics

4.1 Dynamical behaviour of the central core

The core of our network (Figure 2) consists of the antagonist circuit between p53 and nuclear Mdm2, embedded in the 3-element negative circuit involving p53, cytoplasmic and nuclear Mdm2 (denoted P, Mc and Mn, respectively). In this module, p53 acts on two distinct targets. It is unlikely that the thresholds for these two actions are identical. We therefore associate two thresholds with P, which will take the value 0 when its level is below the first threshold, 1 if it is between the first and second threshold, and 2 if it is above the second threshold[1]. In contrast, since cytoplasmic and nuclear Mdm2 are both

[1] Except for the marginal case where both thresholds are identical, in which case p53 takes only the values 0 and 1.

involved in a single action only, Mc and Mn will be treated as binary variables and will take the value 0 for low concentration levels and 1 for high concentration levels. Altogether, only two situations must thus be considered, depending on whether P acts negatively on Mn above its first threshold and positively on Mc above its second threshold, or *vice versa*.

In our graphs P and Mc are both subject to a single control. The logical parameters K_P and $K_{P,\{Mn\}}$ denote the levels that P can reach when its down regulator Mn is below and above its threshold of activity, respectively. We assume that P reaches its upper level if Mn is low and set $K_P = 2$ and $K_{P,\{Mn\}} = 0$. Similarly, we assume that Mc can reach its upper level only if its activator P is present above its relevant activity threshold, and we write $K_{Mc} = 0$ and $K_{Mc,\{P\}} = 1$.

The situation is more complex for nuclear Mdm2. Here, different combinations of its regulators, P and Mc, can influence the level toward which Mn tends to evolve. This is reflected by four logical parameters for Mn: K_{Mn}, $K_{Mn,\{P\}}$, $K_{Mn,\{Mc\}}$, $K_{Mn,\{P, Mc\}}$. These logical parameters have to obey constraints expressing that the negative influence of P tends to lower the level of Mn whereas the positive influence of Mc tends to increase its level. Depending on the relative strength of these two opposite influences, either of two sets of constraints has to be satisfied:

$$K_{Mn,\{P\}} \leq K_{Mn} \leq K_{Mn,\{P, Mc\}} \leq K_{Mn,\{Mc\}} \quad (1.1)$$

or

$$K_{Mn,\{P\}} \leq K_{Mn,\{P, Mc\}} \leq K_{Mn} \leq K_{Mn,\{Mc\}} \quad (1.2)$$

where the equality signs refer to *weak* influences (see Appendix A.1).

Note that as defined in Section 3, these logical parameters represent discretized ratios of the production rates and of the decay rate of nuclear Mdm2, the latter being an increasing function of DNA damage (Stommel and Wahl, 2005). Thus, when DNA damage increases, the decay rate of nuclear Mdm2 will increase and the values of the logical parameters $K_{Mn,\{..\}}$ tend to decrease.

Logical bifurcation analysis

For each choice of the order of the thresholds of P and each one of the inequalities (1.1) and (1.2), one can study the qualitative dynamical properties of the core network as a

function of the degradation rate of nuclear Mdm2. These properties are described by the four "logical bifurcation diagrams" shown in Figure 3.

Let us first consider the situation corresponding to Figure 2(a) where P acts on Mn above its first threshold and on Mc above its second threshold (Figures 3 (a) and (b)).

Starting from a low degradation rate of nuclear Mdm2, on the left, for which all the logical parameters $K_{Mn,\{..\}} = 1$, upon increasing the rate of degradation, successively one logical parameter at the time will switch from 1 to 0, according to the left to right ranking given by inequalities (1.1) or (1.2), until all the logical parameters $K_{Mn,\{..\}} = 0$, at high decay rate. Thus, each column differs from the preceding one by the value of one logical parameter only and each set of parameter values defines a specific dynamical behaviour that can be derived from the logical state tables given in Appendix B.

The bifurcation diagram in Figure 3(a) corresponds to the inequalities (1.1): the positive influence of Mc on the level of Mn is stronger than the negative influence of P. For increasing values of the decay rate of nuclear Mdm2, the system displays successively a stable steady state characterized by a low level of p53 and high level of nuclear Mdm2; the coexistence of this stable state with an oscillatory state; large amplitude cyclic behaviour and finally again a single stable steady state but now with a high level of p53 and low level of nuclear Mdm2.

The first column on the left deals with low decay rates of nuclear Mdm2, whose level is always sufficient to strongly down-regulate the level of p53. None of the feedback circuits is functional. This case models the rest situation in the absence of DNA damage. The second column deals with somewhat higher decay rates of nuclear Mdm2. Here, both feedback circuits become functional: the positive circuit generates a bistable behaviour, while the negative one gives rise to oscillations. This situation may account for the coexistence of cells in the resting state and cells showing sustained p53 oscillations, as observed in the experiments of Geva-Zatorsky et al. (2006). At still higher decay rates of nuclear Mdm2, in the third column, only the negative circuit remains functional and gives rise to a large amplitude cyclic behaviour in agreement with the p53 concentration pulses observed experimentally after irradiation (Geva-Zatorsky et al., 2006; Lahav et al., 2004). Finally, in the fourth column, again none of the circuits is functional. The very high decay rate of nuclear Mdm2 together with the

inhibitory influence of p53 maintains a low level of nuclear Mdm2 so that p53 is steadily high.

The bifurcation diagram in Figure 3(b) gives the sequence of bifurcations when the negative influence of P on the level of Mn is stronger than the positive influence of Mc (cf. inequality (1.2)). This situation favours the positive circuit, which remains the only functional circuit for increasing decay rates of nuclear Mdm2. The third column is now characterized by the coexistence of two stable steady states with, respectively, a low and high level of p53. In particular, the persistence of a steady state with low p53 over a wide range of nuclear Mdm2 degradation rates accounts for the absence of response after irradiation that has been observed experimentally for a fraction of cells by Geva-Zatorsky et al. (2006).

For the situation in Figure 2(b) where P acts on Mc above its lowest threshold and on Mn above its second threshold, two bifurcation scenarios are obtained likewise. They differ from the previous ones by the sequence in which the feedback circuits become functional and generate their characteristic dynamics. When inequality (1.1) prevails, it is now the negative circuit that becomes functional in the first place and it may generate large amplitude p53 oscillations (Figure 3(c)). In the case of inequality (1.2), p53 can reach high levels but there are no large amplitude oscillations, whatever the decay rate of nuclear Mdm2 (Figure 3(d)).

These four logical bifurcation diagrams summarize the qualitative dynamical properties of the core network[1]. They can be understood in terms of the balance between the positive and negative circuit involving p53 as a function of two parameters: the order of the activity thresholds of p53 and the relative strength of the influence of p53 on the level of nuclear Mdm2. These two parameters are related to the binding affinity and transcriptional activity of p53, which are known to be stress- and cell-type specific and dependent on post-translational modifications (Appella and Anderson, 2001; Mayo et al., 2005; Meek, 1998; Feng et al., 2007). Changing one of these parameters at a time allows shifting from one bifurcation scenario to the other and describing different kinds of responses, within the scope of the same interaction network. Such changes in

[1] The marginal case of identical thresholds is also characterized by two bifurcation diagrams. However, the two circuits cannot be functional simultaneously. In the presence of DNA damage, either the negative circuit is operational leading to oscillations, or the positive circuit is operational leading to multistationarity.

parameter values could correspond to different stresses or to differences between individual cells, cell-types or mutational variations.

In the preceding description, the values of the logical parameters associated with P and Mc were kept fixed. Changing their values would account for the behaviour of genetic variants altering the expression of p53 and Mdm2, and allows reproducing the general trends of the experimental observations of Hu et al. (2007). Increasing the basal level of cytoplasmic Mdm2 by fixing $K_{Mc} = K_{Mc,\{P\}} = 1$ leads to the loss of the oscillatory response after irradiation as observed in homozygous cell lines with a single nucleotide polymorphism in the *Mdm2* promoter and over-expressing Mdm2. Modifying the parameter values related to P allows to vary the basal level of p53 and leads to the loss of the oscillatory response when p53 is either under-expressed ($K_P = K_{P,\{Mn\}} = 0$) or over-expressed ($K_P = K_{P,\{Mn\}} = 2$) as observed by Hu et al.(2007) in cell lines expressing p53 under the control of tetracycline.

4.2 Explicit incorporation of DNA damage into the model

The next step consists of including DNA damage explicitly into the model, taking into account that it has a negative influence on the level of nuclear Mdm2 by accelerating its degradation, while high levels of p53 promote damage repair. DNA damage is induced by exposure to stress and will persist unless it is repaired in the presence of p53. The complete graph of interactions is shown in Figure 4 for the situation where P acts on Mn above its first threshold and on Mc above its second threshold[2].

We treat the DNA damage here simply as a two-level discrete variable (Dam), which takes the value 0 when damage is absent (or low) and 1 when damage is present at a significant level. The logical parameters K_{Dam}, $K_{Dam,\{P\}}$ and $K_{Dam,\{P,\,Dam\}}$ take the value 1 during stress induction and 0 otherwise, and $K_{Dam,\{Dam\}} = 1$ ensures that damage decreases only in the presence of p53.

The logical parameters for P and Mc remain as in Section 4.1 since there are no new interactions acting on these variables. For Mn there are now two sets of parameters. The first set of parameters determines the evolution of the level of Mn in the absence of damage and corresponds to the parameters defined for the core network. The second set of parameters determines, now explicitly, the evolution of the level of Mn in the

[2] Note that the introduction of damaged DNA creates a negative three-element circuit between nuclear Mdm2, p53 and DNA damage. However, since DNA damage cannot reappear spontaneously, this negative circuit cannot by itself lead to oscillations.

presence of damage. Taking into account that Dam acts as a down regulator of the level of Mn, the value of these parameters may not exceed those in the absence of damage. Thus, the following constraints have to be obeyed:

$$\begin{aligned} K_{Mn,\{P,\,Dam\}} &\leq K_{Mn,\{P\}} \\ K_{Mn,\{Dam\}} &\leq K_{Mn} \\ K_{Mn,\{P,\,Mc,\,Dam\}} &\leq K_{Mn,\{P,\,Mc\}} \\ K_{Mn,\{Mc,\,Dam\}} &\leq K_{Mn,\{Mc\}} \end{aligned} \tag{2.1}$$

In addition, one has the same type of constraints as already mentioned in the absence of damage:

$$K_{Mn,\{P,\,Dam\}} \leq K_{Mn,\{Dam\}} \leq K_{Mn,\{P,\,Mc,\,Dam\}} \leq K_{Mn,\{Mc,\,Dam\}} \tag{2.2}$$

or

$$K_{Mn,\{P,\,Dam\}} \leq K_{Mn,\{P,\,Mc,\,Dam\}} \leq K_{Mn,\{Dam\}} \leq K_{Mn,\{Mc,\,Dam\}} \tag{2.3}$$

where again, the equality signs refer to *weak* influences. These last two inequalities express, in particular, that nuclear Mdm2 tends to reach its lowest level when its two negative regulators, p53 and DNA damage, are present and the level of cytoplasmic Mdm2 is low.

For each choice of the order of the thresholds of P, these restriction rules limit the number of acceptable combinations of parameter values to 14 possibilities, which describe all the qualitative dynamical potentialities of the network. These dynamical situations can be derived directly from the bifurcation analysis of the core network, taking the inequalities (2.1), (2.2) and (2.3) into account (see Appendix C). For example, if the values of the logical parameters for Mn in the absence of damaged DNA correspond to the first column in Figure 3(a), and the values of the logical parameters in the presence of damage are as in the third column of the same bifurcation diagram, the system will be at rest in a state of low p53 when Dam = 0 and will oscillate when Dam = 1. If instead, the values of the parameters in the presence of damage are those of the fourth column, damage can be repaired through a single p53 peak, without oscillations. This limited number of admissible logical parameter values thus permits an exhaustive qualitative analysis of the model.

For each parameter combination, one can derive the state transition graph, which gives all possible trajectories, stable states and cycles in absence and presence of DNA damage. A typical example for each one of the four bifurcation diagrams of Figure 3 is shown in Figure 5.

Let us consider the state transition graph in Figure 5(a). Here, the positive and negative feedback circuits are both functional when Dam = 0, while only the negative circuit functions when Dam = 1. Starting from the stable rest state [P = 0, Mc = 0, Mn = 1, Dam = 0], a damage inducing stress will shift the system to state (0011) from which it will start to oscillate following one of three possible logical cycles, generating pulses of p53. If the damage can be repaired, the system will leave this cycle (Dam = 0 again) and may either return to its initial stable rest state [0010], or be trapped in a cyclic attractor where P oscillates between 1 and 2. This last situation could indicate that damage cannot be completely repaired and, in normal cells, should lead to apoptosis (Zhang et al., 2007). As described in the next section, which pathway will actually be followed is determined by the values of the time delays representing the rate of evolution of each network component.

Transition graph 5(c) can be understood in a similar way, with the main difference that on one of the logical cycles, in the presence of damaged DNA (Dam = 1), P oscillates continuously between 0 and 1 and never reaches the level that is needed to induce damage repair. This situation would ultimately lead to cell death. On the other hand, if damage is repaired through high p53 pulses, the system eventually goes back to its initial steady state [0010].

In the transition graphs of Figures 5(b) and (d), DNA damage is repaired without oscillations: even a high supply of Mdm2 from the cytoplasm is not able to counteract the negative influence of damage and p53 on the level of nuclear Mdm2, and the negative circuit between P, Mc and Mn cannot function in the presence of damage. Moreover, for the logical parameter values corresponding to Figure 5(d), the initial rest state cannot be restored after damage repair and the system remains caught in a steady state with high levels of p53 and cytoplasmic Mdm2, which could correspond to a damage-induced dysfunctioning of the p53-Mdm2 network[3].

[3] As a matter of fact, in the case of Figure 5(b), none of the feedback circuits is functional while in the case of Figure 5(d), the positive circuit generates two stable steady states in the absence of DNA damage.

4.3 Simulation of single cell and cell population dynamics

Once the logical parameter values are fixed, the pathway the system will actually follow, among all the possible pathways in a state transition graph, is determined by conditions on the "on" and "off" time delays associated with each variable of the network. These delays represent the time between the moment a signal is given to a variable to increase or decrease and the moment where a significant change in its level will effectively be achieved. In the case of a branching point, the state that will be reached is the one requiring the least time from the state where the signal has initially been given. For example, in Figure 5(a), the signal for damage repair (P = 2) is given at state 2001. One will go from state 2001 to 2101 if the time required to switch variable Mc on is shorter than the time needed for damage repair, i.e. $t_{Mc} < t_{\overline{Dam}}$, and to state 2000 otherwise. At state 2101, a new choice appears. Since the signal (Mc = 1) to switch on variable Mn has just been given, while the signal for damage repair has already been given one step ahead, the decision to switch from 2101 to 2100 or to 2111 now depends on the relative values of $t_{\overline{Dam}}$ and $t_{Mc} + t_{Mn}$. At this bifurcation point, state 2111 will occur if $t_{\overline{Dam}} > t_{Mc} + t_{Mn}$ and state 2100 otherwise. In this way, the constraints on the values of the time delays that have to be obeyed for traversing a given pathway can be derived from the successive branching decisions (see, for example, Table 1). Thus, for a given set of logical parameters, a choice of time delays will fully determine the evolution of the system.

It is important to note that the time delays may combine several factors and may represent completely different processes for different variables. For example, the increase in the level of cytoplasmic Mdm2 is linked to the activation of gene *Mdm2* by the p53 protein. The "on" delay for Mc thus represents the transcription of gene *Mdm2*, the translocation of Mdm2 mRNA to the cytoplasm and its translation into proteins. The increase in the level of nuclear Mdm2, on the other hand, is linked to the translocation of protein Mdm2 from the cytoplasm into the nucleus, and the "on" delay for Mn combines the phosphorylation and translocation of cytoplasmic Mdm2. Therefore, these two "on" delays will presumably have different values as will also be the case for most of the other time delays.

Let us focus on the transition graph in Figure 5(a), which captures the oscillations observed experimentally and exhibits a rich variety of behaviour. As one can see, in the

presence of DNA damage, p53 can oscillate by following one of three different logical cycles (lc) labelled 1A, 1B and 1C. The conditions that have to be satisfied to follow either of these cyclic pathways are presented in Table 2 and involve the decay rates of p53, cytoplasmic and nuclear Mdm2.

The system will oscillate as long as DNA damage is present or, in logical terms, as long as the cycling condition:

$$t_{\overline{Dam}} > t_{Mc} + t_{Mn} + t_{\overline{P(2)}}$$

remains satisfied (where $t_{\overline{P(2)}}$ represents the time needed for P to decrease from level 2 to 1).

Modelling the damage repair

Each burst of p53, however, will lead to the repair of a certain amount of DNA damage. To transpose this into our logical modelling, we have to define a progressive decrease of a quantity associated with damage repair. We have ascribed to the damage variable the values 0 or 1, meaning that damage is absent (or low) or significantly present but its exact level is not specified. A decrease from 1 to 0 of the damage in just one burst could thus represent a very important repair. Instead, we reason that the higher the damage, the more time it needs to be repaired and propose the following ansatz: the delay $t_{\overline{Dam}}$ associated with the disappearance of the damage decreases by a certain amount τ after each p53 burst. Thus :

$$t_{\overline{Dam}}(n) = t^{0}_{\overline{Dam}} - n.\tau \geq 0$$

where n is the number of p53 bursts. At the start, when damage is created, n = 0 and it increases by 1 at each turn. So after each p53 burst the delay associated with the disappearance of the damage is reduced by a certain amount that accounts for the efficiency of the repair machinery, until one of the conditions a, b or c in Table 1 is no longer fulfilled. In this way the number of oscillations that are needed by the system to eliminate the damage will depend on the initial damage (the initial time delay $t^{0}_{\overline{Dam}}$) and the efficiency of the repair process (the amount τ by which the delay is reduced with each oscillation).

One can reason in a similar way for the off time delay associated with Mn. Since the degradation rate of nuclear Mdm2 is an increasing function of the damage level, the

higher the damage the faster the level of this protein decays. Therefore, we set the time delay for the disappearance of Mn:

$$t_{\overline{Mn}}(n) = t^{b}_{\overline{Mn}} - t^{0}_{\overline{Mn}} \cdot \frac{t_{\overline{Dam}}(n)}{t^{0}_{\overline{Dam}}} > 0$$

where $t^{b}_{\overline{Mn}}$ is the off time delay when there is no damage (low basal degradation rate of nuclear Mdm2); $t^{0}_{\overline{Mn}}$ is a function of the initial damage level after irradiation and $t_{\overline{Dam}} / t^{0}_{\overline{Dam}}$ accounts for the amount of damage that is repaired with each oscillation. In this way, the time delay $t_{\overline{Mn}}$ will shorten in presence of DNA damage and progressively return to its basal value when damage is eliminated (Stommel and Wahl, 2005). Note that context sensitive time delays have also recently been considered by Siedbert and Bockmayr (2007; 2008).

After repair, the system will either return to its initial steady state [0010] or display low frequency oscillations corresponding to the logical cycle lc 2, depending on the values of the time delays (see Tables 1 and 2).

Single cell simulations

Figure 6 shows deterministic simulations of the time evolution of p53 in an individual cell after a damage inducing stress, for different initial damage levels and repair efficiencies. Except for $t_{\overline{Dam}}$ and $t_{\overline{Mn}}$, which reflect the decreasing level of damage, each time delay has a fixed value and the set of values of the delays impose a well-defined pathway.

For a low initial damage, the system follows cycle 1B corresponding to large amplitude and rather low frequency p53 oscillations (Figure 6(a)). The corresponding evolution of the time delay associated with the disappearance of damage is shown in Figure 6(b). After complete repair the system settles back in the steady state with a low level of p53 and high level of nuclear Mdm2.

For a high initial damage and the same repair rate, the system oscillates on cycle 1C as long as the damage remains high. These oscillations are characterized by a smaller amplitude but higher frequency and mean level of p53 (Figure 6(c) and (d)). When the level of damage has sufficiently decreased, one observes a shift towards large amplitude and lower frequency oscillations, corresponding to the passage from cycle 1C to 1B. If one increases the rate of repair, however, high initial damage levels lead to the same

type of response as low damage levels (Figure 6(e) and (f)).

The case of lasting p53 oscillations despite damage repair is illustrated in Figure 7. The system oscillates on cycle 1C in the presence of a high damage level and presents slower but sustained oscillations (on cycle 2) even after most of the damage has been repaired. Whether this last situation corresponds to a pathological case remains to be determined. Note, however, that as shown below, these oscillations turn out not to be very robust when stochastic effects are taken into account.

The situation is somewhat different for the case of the state transition graph 5(c), which also accounts for the generation of p53 pulses in the presence of damage. A common feature with previous case is the presence of three embedded logical cycles when there is damaged DNA. However, the conditions that determine which of these cyclic pathways will be followed now involve the production rates of p53, cytoplasmic and nuclear Mdm2 rather than their decay rates. In particular, if the time needed for accumulating p53 to level 2 is high, p53 may oscillate permanently between 0 and 1 and be unable to induce damage repair. On the other hand, if damage is repaired through large amplitude oscillations, the system will always return to the rest state [0010].

Cell population simulations

In a population of cells, different cells will have slightly different internal characteristics and may acquire a more or less severe damage upon exposure to stress. Moreover, in each individual cell, the rate of the different processes may fluctuate in time. We therefore ascribe to each time delay a distribution centred on a mean value (Thomas, 1979) and, for each simulation, each time a variable has a call to switch, the corresponding time delay is drawn at random from its distribution. The behaviour of a cell population is then modelled by averaging over a number of simulations, each simulation representing an individual cell. For sake of simplicity, we have chosen a square distribution with a standard deviation of 10% of the mean for every time delay, including $t^{0}_{\overline{Dam}}$ and τ, which seems reasonable to account for differences between cells.

The following simulations were performed for the case corresponding to Figure 5(a) and for a population of 100 cells. We first chose a set of average values of the delays such that starting from steady state [0010], after irradiation, every cell follows cycle 1B and returns to the steady state after repair. In Figure 8(a) one can see damped p53 oscillations at the level of the cell population. In addition to phase shifts between the

cells, dampening is here mainly caused by the fact that the initial damage level (t^{0}_{Dam}) is not identical for all cells and that some cells repair the damage faster than others, thus leading to fewer p53 bursts. The dampening is however slow.

In Figure 8(b), the average values of the time delays are such that the cells have the possibility to follow different cycles with different amplitudes and frequencies. Upon repair the cells can either return to the steady state or remain trapped on cycle 2. However, due to fluctuations in the time delays, these residual oscillations disappear sooner or later, and all cells stabilize again in state [0010]. One observes now a faster and stronger dampening of the population response, with wider and progressively smaller peaks, in good agreement with experimental observations (Bar-Or et al., 2000; Hamstra et al., 2006). See also Ma et al., (2005). Note that larger values of the standard deviations will increase the noise in the system and may lead to a faster dampening of the oscillations at the population level, while for lower values the behaviour becomes closer to the deterministic one. However, for a wide range of standard deviations, the results remain qualitatively similar to those shown here.

5. From logical to differential description

It is now recognized that logical descriptions are in good qualitative agreement with piecewise-linear differential systems or differential systems with steep sigmoids (Glass and Kauffman, 1973; Kaufman et al., 1985; Snoussi, 1989). One may ask, however, whether the qualitative features of the dynamics are still preserved when relaxing the high nonlinearity inherent to the logical treatment and introducing a more realistic and detailed description of the interactions. Therefore, we have translated our logical model into the following set of four ordinary differential equations, in which the nonlinearities are Hill functions with an exponent n = 4 only:

$$
\begin{aligned}
\frac{\mathrm{d}P}{\mathrm{d}t} &= k_P \frac{K_P^4}{1+Mn^4} - \left(d_P + d'_P Mn\right)\cdot P \\
\frac{\mathrm{d}Mc}{\mathrm{d}t} &= k_{Mc} + k'_{Mc}\frac{P^4}{K_{Mc}^4 + P^4} - \left(k_{in} - k'_{in}\frac{P^4}{1+P^4}\right)\cdot Mc + \frac{1}{V_r}k_{out}Mn - d_{Mc}Mc \\
\frac{\mathrm{d}Mn}{\mathrm{d}t} &= V_r\left(k_{in} - k'_{in}\frac{P^4}{1+P^4}\right)\cdot Mc - k_{out}Mn - d_{Mn}Mn \\
\frac{\mathrm{d}Dam}{\mathrm{d}t} &= k_{IR}\cdot IR - k_{Dam}\frac{P^4}{K_{Dam}^4 + P^4}\cdot Dam
\end{aligned}
\qquad (3)
$$

where $d_{Mn} = d'_{Mn} + d''_{Mn} \frac{Dam}{K_{Mn} + Dam}$.

In these equations, nuclear Mdm2 down regulates the level of active p53 both by blocking its accumulation and by accelerating its degradation. p53 participates in a number of steps involving transcriptional activity. Since it binds to DNA mainly under the form of a tetramer (Chène, 2001; Friedman et al., 1993; McLure and Lee, 1998; Weinberg et al., 2004), we assume that it enhances Mdm2 transcription following a Hill function with exponent n = 4, and similarly for the down regulation of the translocation of Mdm2 and the induction of DNA damage repair. Moreover, since DNA damage activates ATM, a kinase involved in Mdm2 destabilization, through intermolecular autophosphorylation (Bakkenist and Kastan, 2003), the acceleration of Mdm2 degradation by DNA damage is also represented by a non-linear process.

We have analyzed the bifurcation properties of this differential model as a function of three key parameters closely related to our logical analysis:

- the degradation rate of nuclear Mdm2, d_{Mn}, which has been used to construct the logical bifurcation diagrams given in Figure 3,
- the strength of the negative influence of p53 on the nuclear translocation of cytoplasmic Mdm2, k'_{in}, which determines which of the two logical constraints (1.1) or (1.2) is satisfied, and
- the DNA-binding affinity of p53, K_{Mc}, which represents (in our normalized equations) the ratio between the concentration thresholds associated with the influence of p53 on cytoplasmic and nuclear Mdm2. In other words, K_{Mc} is related to the order of the thresholds associated with variable P in the logical modeling (see Section 4.1).

Of note, K_{Mc} is stress-, cell- and tissue-specific, since p53 is known to be subject to several context-dependent post-translational modifications that can strongly modify its DNA binding properties and affect its transcriptional activity (Appella and Anderson, 2001; Brooks and Gu, 2003; Meek, 1998). Moreover, the influence of p53 in the down-regulation of nuclear translocation of cytoplasmic Mdm2, *via* the Akt kinase, has also been shown to be stress and cell-type specific (Feng et al., 2007; Mayo et al., 2005).

A detailed analysis of this differential model will be presented elsewhere (manuscript in preparation). Here, we show that even though the continuous description using

moderate nonlinearities generates some additional dynamical properties, the essential features of the dynamics still fit with the predictions of our logical analysis. One can easily find pairs of (K_{Mc}, k'_{in}) values for the differential system that lead to bifurcation diagrams comparable to the four logical bifurcation diagrams shown in Figure 3 (see Figure S1, supplementary material). Moreover, as in the logical modelling, our continuous model accounts for the loss of oscillations for high basal production rates of Mdm2 as well as for high and low production rates of p53 (Figure S2, supplementary material), in agreement with the observations of Hu et al. (2007) and Ma et al. (2005).

Let us here, for example, consider the case where K_{Mc} is high and the negative influence of p53 on nuclear Mdm2 is weak, which in logical terms corresponds to the conditions of Figure 3(a). In the differential description these conditions can be satisfied by a whole spectrum of values of K_{Mc} and k'_{in}. Figure 9 presents a sequence of three typical bifurcation diagrams that are globally in very good agreement with the corresponding logical situation.

For K_{Mc} = 15 (weak affinity of p53 for *Mdm2*), as d_{Mn} increases, the differential model displays successively a stable steady state with a low level of p53, the coexistence of this stable steady state with an oscillatory state, a stable oscillatory state, and finally a stable steady state with high levels of p53. Note that, due to the lowering of the nonlinearities, there appears here a small region of coexistence of two stable steady states at low d_{Mn}, just before the emergence of oscillations.

For lower values of K_{Mc}, the oscillatory regime breaks up through infinite period bifurcations giving rise to long period oscillations and bi-cyclic behaviour. In particular for K_{Mc} = 5 (higher affinity of p53 for *Mdm2*), the general bifurcation picture remains consistent with the logical model with, as d_{Mn} increases, a stable steady state with a low level of p53 followed successively by an oscillatory domain and a stable steady state with high p53 level. This sequence of dynamical behaviour is similar to the bifurcation sequence shown in Ciliberto et al. (2005). Here, however, one finds in the oscillatory domain a region of coexistence of two stable limit cycles of significantly different periods and mean levels (Figure 10). This has several implications. In particular, this bi-cyclicity renders the system very sensitive to the level of damage and efficiency of damage repair. For low DNA damage (not shown), one observes large amplitude oscillations of low frequency and mean level whatever the damage repair rate (k_{Dam}),

while for high DNA damage the situation strongly depends on k_{Dam}. More precisely, when damage is high and the repair rate low, one observes oscillations of high frequency and mean level as long as the damage is high, with a shift to low frequency oscillations when damage progressively disappears (Figure 11(a)). But, when the repair rate is high, damage is rapidly repaired with large amplitude oscillations of low frequency (Figure 11(b)), as well predicted by the logical model. Interestingly, one observes that the ratio of the periods of the two oscillatory regimes is close to two (see Figure 10), in good agreement with experimental data (see Figure S3 in Geva-Zatorsky et al., 2006). These results may contribute to the understanding of the frequency tuning that is observed as a function of the irradiation dose and predict that the rate of damage repair should play an important role for this behaviour.

6. Conclusion

In this paper, we have studied a simple model of the p53-Mdm2 network first using a logical approach. This structure-oriented approach allows an extensive analysis of the dynamical potentialities of the network on the basis of the "functionality" of its constitutive feedback circuits (generation of multistationarity for positive circuits, homeostasis and oscillations for negative circuits) rather than focusing on the individual interactions. It enables a rigorous investigation of the relative importance of the positive and negative feedback circuits composing the network for the dynamical behaviour of the system. However, one has to note that the abstraction to discrete levels and the high inherent nonlinearity of this method restricts us to qualitative results.

New developments of the logical method have been introduced: first, the concept of logical bifurcation diagram, which describes the changes in the dynamics of the system as a function of a quantity linked to the logical parameters of the model. Here, the logical parameters describing the strength of the interactions acting on nuclear Mdm2 are all implicitly linked to its degradation rate that increases with the level of DNA damage. Provided the network connectivity remains low, extension to large systems may be possible. Secondly, on/off time delays that may vary in time have been used for describing the deterministic or stochastic dynamics of single cells and cell populations in the logical framework.

Applying these logical tools, we show that the main dynamical properties of our network can be summarized by only four logical bifurcation diagrams as a function of the damage level. These bifurcation scenarios differ by the sequence in which the

feedback circuits generate their characteristic dynamics and depend on the binding affinity and transcriptional activity of p53, underlining the role of these two parameters for the behaviour of the network. Since these parameters are known to be related to the post-translational modifications of protein p53, which are stress- and cell-type specific, we propose that different cell- or stress-types could be characterized by different bifurcation schemes and lead to different responses after irradiation. Furthermore, these differences in behaviour can be understood in terms of the balance between the intertwined positive and negative feedback circuits involving p53. When the negative circuit is favoured, oscillatory responses prevail. When the positive circuit is favoured, multistability predominates, leading to an all-or-none type of behaviour with either a very weak or no response upon irradiation or a strong response at very high damage levels.

Although our picture of the p53-Mdm2 network is very simplified, our logical modeling accounts for the variability of dynamical behaviour observed experimentally (Geva-Zatorsky et al., 2006). By simulating the time evolution of single cells and cell populations in the framework of the bifurcation scenario presented in Figure 3(a), we can qualitatively reproduce several features of the p53 response to damage such as p53 pulses after irradiation, persistent oscillations, shifts in the frequency of the oscillations in the course of the response, or rapid dampening of the oscillations in a cell population. We also show that the response of our system is very sensitive to the level of damage and efficiency of damage repair.

In a next step, we have translated our logical model into a set of differential equations, keeping only moderate nonlinearities and introducing realistic parameter values. The essential behaviours found in the logical context are conserved, showing that the structure of the network determines its main dynamical potentialities, to a large extent independently of the mechanistic details.

An important feature of our differential model is the existence, as a function of the damage level, of two oscillatory regimes of significantly different periods and mean levels, separated by a cyclic fold. This result provides an attractive interpretation of the short and long characteristic periods of oscillation reported by Geva-Zatorsky et al. (2006) depending on the irradiation doses (see Figures 3 and S3 in this reference). This behaviour, which has not been accounted for in other modeling approaches, will be further analyzed in a following paper, more focused on the differential and stochastic

descriptions of our model. As to the physiological role of these two different oscillatory modes, differences in the frequency and mean level of the p53 oscillations might provide a mechanism for encoding the damage severity and allow for differential activation of genes involved in DNA repair and apoptosis.

Acknowledgements:

We wish to thank R. Thomas for critical reading of the manuscript and F. Vikas for his help at early stages of this work. We acknowledge financial support from a EU STREP Grant (COMBIO) and the Communauté Française de Belgique (ARC Grant 04/09-307).
The logical analysis has been performed in part with the freely available logical software SMBioNet (http://smbionet.lami.univ-evry.fr/) and GINsim (http://gin.univ-mrs.fr/), and the bifurcation analysis with XPPAUT (http://www.math.pitt.edu/~bard/xpp/xpp.html).

Appendix A

A.1 Strong and weak interactions in the logical description

The strength of an interaction in the discrete framework is illustrated in Figure A.1, in the case where a variable y activates (*top*) or represses (*bottom*) a variable x. k_x and $k_{x,\{y\}}$ represent the ratio of the rates of production and decay of x when y is below and above its relevant threshold of activity, respectively. The corresponding logical parameters K_x and $K_{x,\{y\}}$ are the discretized values of these ratios according to the logical scale. They specify the integer value toward which x tends to evolve when y is below or above its relevant threshold of activity. In the case of a weak activation, $k_{x,\{y\}}$ and k_x are both below the threshold s_1 and $K_x = K_{x,\{y\}} = 0$. In the case of a strong interaction, $k_{x,\{y\}}$ is now above threshold s_1 and $K_x = 0$ and $K_{x,\{y\}} = 1$. In the case of a weak repression, $k_{x,\{y\}}$ and k_x are both above s_1 and $K_x = K_{x,\{y\}} = 1$. In the case of a strong repression, $k_{x,\{y\}}$ is now below s_1 and $K_x = 1$ and $K_{x,\{y\}} = 0$.

A.2 Circuit functionality

To each feedback circuit one can associate a characteristic state, which is the state located at the threshold of action of the variables involved in the circuit. Snoussi and Thomas (1993) have shown that whenever a circuit-characteristic state is steady, the circuit will be functional and generate its characteristic dynamical properties. Reciprocally, whenever a circuit is functional, its characteristic state is steady. The

procedure to identify if a circuit-characteristic state is steady can be found in Snoussi and Thomas (1993). These particular states thus play an essential role in the dynamics of a system, and the generalized logical method allows determining the parameter constraints in order for any combination of circuits to be functional.

The notions of circuit functionality and characteristic state are here illustrated in Figure A.2 for the positive circuit of the core network, in the case where P acts on Mn above its lowest threshold (Panel (a)). This situation corresponds to the interaction graph of Figure 2 (a). In Panel (b), left, Mn has a strong influence on the level of P (K_P = 2 and $K_{P,\{Mn\}}$ = 0) but P has only a weak influence on Mn ($K_{Mn} = K_{Mn,\{P\}}$ = 1). The positive circuit is not functional and there is only one stable steady state (*black circle*). When both P and Mn have a strong influence on each other, the circuit is functional and gives here rise to multistationarity (Panel (b), right). The two stable steady states (*black circles*) are separated by the characteristic state [$s_P^{(1)}$ $s_{Mn}^{(1)}$] of the circuit (*open circle*). We call steady state [$s_P^{(1)}$ $s_{Mn}^{(1)}$] an *unstable steady state* because in continuous descriptions the steady states that are characteristic of positive circuits are located on separatrices and always unstable (Snoussi and Thomas, 1993; Thomas et al., 1995, Thomas and Kaufman, 2001b).

Appendix B

Parametric state tables for the core network

For each set of logical parameter values associated with Mn, the stable logical states and cycles are derived from state table B.1 (a), when P acts on Mn above its first threshold, and from state table B.1 (b), when P acts on Mn above its second threshold. The logical parameter values for P and Mc are defined in section 4.1.

Appendix C

Derivation of the acceptable parameter sets for nuclear Mdm2 (Mn)

When DNA damage is incorporated into the model, for each choice of the order of the thresholds of P, the restriction rules (2.1), (2.2) and (2.3) limit the number of acceptable combinations of logical parameter values for Mn to 14 possibilities. These combinations can be derived directly from the bifurcation analysis of the core network. According to inequalities 2.1, the logical parameters $K_{Mn,\{\ldots,Dam\}}$, in the presence of damage, are only allowed to take the same values as those in the absence of damage or values

corresponding to one of the next columns of the two bifurcation diagrams compatible with the threshold order of P. When P acts on Mn above its first threshold, the 14 acceptable combinations of parameters can thus be derived as follows:

1. If the set of values of the logical parameters for Mn in the absence of damaged DNA corresponds to the first column in Figure 3(a), there are 5 accessible sets of values for the logical parameters in the presence of damage, corresponding to Figure 3(a) column 1, 2, 3, 4 and Figure 3(b) column 3;

2. If the set of values of the logical parameters for Mn in the absence of damaged DNA corresponds to the second column in Figure 3(a), there are 4 accessible sets of values for the logical parameters in the presence of damage, corresponding to Figure 3(a) column 2, 3, 4 and Figure 3(b) column 3;

3. If the set of values of the logical parameters for Mn in the absence of damaged DNA corresponds to the third column in Figure 3(a), there are 2 accessible sets of values for the logical parameters in the presence of damage, corresponding to Figure 3(a) column 3 and 4;

4. If the set of values of the logical parameters for Mn in the absence of damaged DNA corresponds to the fourth column in Figure 3(a), there is only one accessible set of values for the logical parameters in the presence of damage, corresponding to Figure 3(a) column 4;

5. Finally, if the set of values of the logical parameters for Mn in the absence of damaged DNA corresponds to the third column in Figure 3(b), there are 2 accessible sets of values for the logical parameters in the presence of damage, corresponding to Figure 3(b) column 3 and 4.

The same counting rule is applied to derive the 14 possibilities when P acts on Mn above its second threshold, using Figure 3(c) and 3(d).

Note that some parameter combinations lead to a very similar qualitative behaviour and only differ by details in the state transitions. Moreover, for each threshold order of P, five among the 14 admissible parameter combinations correspond to a weak influence of Dam: the parameter values as well as the dynamical properties are similar in the absence or presence of damage. This further reduces the total number of qualitative distinct situations to consider to about ten.

References

Adimoolam, S., and Ford, J. M., 2003. p53 and regulation of DNA damage recognition during nucleotide excision repair. DNA Repair (Amst) 2 (9), pp. 947-954.

Appella, E., and Anderson, C. W., 2001. Post-translational modifications and activation of p53 by genotoxic stresses. Eur. J. Biochem. 268 (10), pp. 2764-2772.

Bakkenist, C. J., and Kastan, M. B., 2003. DNA damage activates ATM through intermolecular autophosphorylation and dimer dissociation. Nature 421 (6922), pp. 499-506.

Barak, Y., Juven, T., Haffner, R., and Oren, M., 1993. Mdm2 expression is induced by wild type p53 activity. EMBO J. 12 (2), pp. 461-468.

Bar-Or, R. L., Maya, R., Segel, L. A., Alon, U., Levine, A. J., and Oren, M., 2000. Generation of oscillations by the p53-Mdm2 feedback loop: a theoretical and experimental study. Proc. Natl. Acad. Sci. USA 97 (21), pp. 11250-11255.

Batchelor, E., Mock, C. S., Bhan, I., Loewer, A. and Lahav, G.,2008. Recurrent initiation: a mechanism for triggering p53 pulses in response to DNA damage. Mol. Cell 30 (3), pp. 277-289.

Bose, I., and Ghosh, B., 2007. The p53-MDM2 network: from oscillations to apoptosis. J. Biosci. 32 (5), pp. 991-997.

Bottani, S., and Grammaticos, B., 2007. Analysis of a minimal model for p53 oscillations. J. Theor. Biol. 249 (2), pp. 235-245.

Brooks, C. L., and Gu, W., 2006. p53 ubiquitination: Mdm2 and beyond. Mol. Cell 21 (3), pp. 307-315.

Brooks, C. L., and Gu, W., 2003. Ubiquitination, phosphorylation and acetylation: the molecular basis for p53 regulation. Curr. Opin. Cell. Biol. 15 (2), pp. 164-171.

Chen, J., Lin, J., and Levine, A. J., 1995. Regulation of transcription functions of the p53 tumor suppressor by the mdm-2 oncogene. Mol Med 1 (2), pp. 142-152.

Chène, P., 2001. The role of tetramerization in p53 function. Oncogene 20 (21), pp. 2611-2617.

Chickarmane, V., Nadim, A., Ray, A., and Sauro, H. M., 2005. A p53 Oscillator Model of DNA Break Repair Control. arXiv:q-bio/0510002. Available at http://www.citebase.org/abstract?id=oai:arXiv.org:q-bio/0510002

Ciliberto, A., Novak, B., and Tyson, J. J., 2005. Steady states and oscillations in the p53/Mdm2 network. Cell Cycle 4 (3), pp. 488-493.

Coutts, A. S., Boulahbel, H., Graham, A. and Thangue, N. B. L., 2007. Mdm2 targets the p53 transcription cofactor JMY for degradation. EMBO Rep. 8 (1), pp. 84-90.

Fauré, A., Naldi, A., Chaouiya, C., Thieffry, D., 2006. Dynamical analysis of a generic Boolean model for the control of the mammalian cell cycle, Bioinformatics 22(14), pp. e124-e131.

Fei, P., Bernhard, E. J., and El-Deiry, W. S., 2002. Tissue-specific induction of p53 targets in vivo. Cancer Res. 62 (24), pp. 7316-7327.

Feng, L., Lin, T., Uranishi, H., Gu, W., and Xu, Y., 2005. Functional analysis of the roles of posttranslational modifications at the p53 C terminus in regulating p53 stability and activity. Mol. Cell Biol. 25 (13), pp. 5389-5395.

Feng, Z., Hu, W., Stanchina, E. d., Teresky, A. K., Jin, S., Lowe, S., et al., 2007. The regulation of AMPK beta1, TSC2, and PTEN expression by p53: stress, cell and tissue specificity, and the role of these gene products in modulating the IGF-1-AKT-mTOR pathways. Cancer Res. 67 (7), pp. 3043-3053.

Freedman, D. A., Wu, L., and Levine, A. J., 1999. Functions of the MDM2 oncoprotein. Cell Mol. Life Sci. 55 (1), pp. 96-107.

Friedman, P. N., Chen, X., Bargonetti, J., and Prives, C., 1993. The p53 protein is an unusually shaped tetramer that binds directly to DNA. Proc. Natl. Acad. Sci. USA 90 (8), pp. 3319-3323.

Gatz, S. A. and Wiesmüller, L., 2006. p53 in recombination and repair, Cell Death Differ., 13 (6), pp. 1003-1016.

Geva-Zatorsky, N., Rosenfeld, N., Itzkovitz, S., Milo, R., Sigal, A., Dekel, E., et al., 2006. Oscillations and variability in the p53 system. Mol. Syst. Biol., 2, 2006.0033.

Glass, L. and Kauffman, S. A., 1973. The logical analysis of continuous, nonlinear biochemical control networks, J. Theor. Biol., 39, pp. 103-129.

Gonzalez, A. G., Naldi, A., Sánchez, L., Thieffry, D., Chaouiya, C., 2006, GINsim: a software suite for the qualitative modelling, simulation and analysis of regulatory networks., *Biosystems* 84(2), pp. 91-100.

Gottlieb, T. M., Martinez, J. F., Seger, R., Taya, Y., and Oren, M., 2002. Cross-talk between Akt, p53 and Mdm2: possible implications for the regulation of apoptosis. Oncogene 21 (8), pp. 1299-1303.

Hamstra, D. A., Bhojani, M. S., Griffin, L. B., Laxman, B., Ross, B. D., and Rehemtulla, A., 2006. Real-time evaluation of p53 oscillatory behavior in vivo using bioluminescent imaging. Cancer Res. 66 (15), pp. 7482-7489.

Haupt, Y., Maya, R., Kazaz, A., and Oren, M., 1997. Mdm2 promotes the rapid degradation of p53. Nature 387 (6630), pp. 296-299.

Honda, R., and Yasuda, H., 2000. Activity of MDM2, a ubiquitin ligase, toward p53 or itself is dependent on the RING finger domain of the ligase. Oncogene 19 (11), pp. 1473-1476.

Hu W., Feng Z., Ma L., Wagner J., Rice J.J., Stolovitzky G., Levine A.J., 2007. A single nucleotide polymorphism in the MDM2 gene disrupts the oscillation of p53 and MDM2 levels in cells. Cancer Res. 67 (6), pp. 2757-2765.

Kaufman, M., Urbain, J. and Thomas, R., 1985. Towards a logical analysis of the immune response, J. Theor. Biol. 114, pp. 527-561.

Lahav, G., Rosenfeld, N., Sigal, A., Geva-Zatorsky, N., Levine, A. J., Elowitz, M. B., et al., 2004. Dynamics of the p53-Mdm2 feedback loop in individual cells. Nat. Genet. 36 (2), pp. 147-150.

Lozano, G., and Elledge, S. J., 2000. p53 sends nucleotides to repair DNA. Nature 404 (6773), pp. 24-25.

Ma, L., Wagner, J., Rice, J. J., Hu, W., Levine, A. J., and Stolovitzky, G. A., 2005. A plausible model for the digital response of p53 to DNA damage. Proc. Natl. Acad. Sci. USA 102 (40), pp. 14266-14271.

Mayo, L. D., and Donner, D. B., 2002. The PTEN, Mdm2, p53 tumor suppressor-oncoprotein network. Trends Biochem. Sci. 27 (9), pp. 462-467.

Mayo, L. D., Seo, Y. R., Jackson, M. W., Smith, M. L., Guzman, J. R., Korgaonkar, C. K., et al., 2005. Phosphorylation of human p53 at serine 46 determines promoter selection and whether apoptosis is attenuated or amplified. J. Biol. Chem. 280 (28), pp. 25953-25959.

McLure, K. G., and Lee, P. W., 1998. How p53 binds DNA as a tetramer. EMBO J. 17 (12), pp. 3342-3350.

Meek, D. W., 1998. Multisite phosphorylation and the integration of stress signals at p53. Cell Signal 10 (3), pp. 159-166.

Momand, J., Zambetti, G. P., Olson, D. C., George, D., and Levine, A. J., 1992. The mdm-2 oncogene product forms a complex with the p53 protein and inhibits p53-mediated transactivation. Cell 69 (7), pp. 1237-1245.

Monk, N. A., 2003. Oscillatory Expression of Hes1, p53, and NF-kappa B Driven by Transcriptional Time Delays. Current Biology 13, pp. 1409-1413.

Naldi, A., Thieffry, D., Chaouiya, C., (2007). Decision diagrams for the representation of logical models of regulatory networks. In CMSB'07, Lecture Notes In Bioinformatics (LNBI) 4695, pp. 233-247.

Offer, H., Wolkowicz, R., Matas, D., Blumenstein, S., Livneh, Z., and Rotter, V., 1999. Direct involvement of p53 in the base excision repair pathway of the DNA repair machinery. FEBS Lett. 450 (3), pp. 197-204.

Ogunnaike, B. A., 2006. Elucidating the digital control mechanism for DNA damage repair with the p53-Mdm2 system: single cell data analysis and ensemble modelling. J. R. Soc. Interface 3 (6), pp.175-184.

Oliner, J. D., Pietenpol, J. A., Thiagalingam, S., Gyuris, J., Kinzler, K. W., and Vogelstein, B., 1993. Oncoprotein MDM2 conceals the activation domain of tumour suppressor p53. Nature 362 (6423), pp. 857-860.

Oren, M., 2003. Decision making by p53: life, death and cancer. Cell Death Differ. 10 (4), 2003, pp. 431-442.

Oren, M., Damalas, A., Gottlieb, T., Michael, D., Taplick, J., Leal, J. F. M., Maya, R., Moas, M., Seger, R., Taya, Y. and Ben-Ze'ev, A., 2002. Regulation of p53: intricate loops and delicate balances. Biochem. Pharmacol. 64 (5-6), pp. 865-871.

Puszyński, K., Hat, B., and Lipniacki, T., 2008. Oscillations and bistability in the stochastic model of p53 regulation. J. Theor. Biol. 254 (2), pp. 452-465.

Ramalingam, S., Honkanen, P., Young, L., Shimura, T., Austin, J., Steeg, P. S., Nishizuka, S., 2007. Quantitative assessment of the p53-Mdm2 feedback loop using protein lysate microarrays., Cancer Res 67(13), pp. 6247-6252.

Remy, E., Ruet, P., Thieffry, D., 2008. Graphic requirements for multistability and attractive cycles in a Boolean dynamical framework. Advances in Applied Mathematics 41, pp. 335-350.

Richard, A., Comet, J.-P., 2007. Necessary conditions for multistationarity in discrete dynamical systems. Discrete Applied Mathematics, 155(18), pp. 2403-2413.

Siedbert, H., Bockmayr, A., 2007. Context Sensitivity in Logical Modelling with Time Delays. Computational Methods in Systems Biology, CMSB 2007. Springer, LNBI 4695, pp. 64-79.

Siedbert, H., Bockmayr, A., 2008, Temporal Constraints in the Logical Analysis of Regulatory Networks. Theoretical Computer Science, 391, pp. 258-275.

Singh, B., Reddy, P. G., Goberdhan, A., Walsh, C., Dao, S., Ngai, I., et al., 2002. p53 regulates cell survival by inhibiting PIK3CA in squamous cell carcinomas. Genes Dev. 16 (8), pp. 984-993.

Snoussi, E. H., 1989. Qualitative dynamics of piecewise-linear differential equations: a discrete mapping approach. Dynamics and Stability of Systems 4, pp. 189-207.

Snoussi, E. H. and Thomas, R., 1993. Logical identification of all steady states: the concept of feedback loop characteristic states. Bull. Math. Biol. 55, pp. 973-991.

Stambolic, V., MacPherson, D., Sas, D., Lin, Y., Snow, B., Jang, Y., et al., 2001. Regulation of PTEN transcription by p53. Mol Cell, 8, pp. 317-325.

Stommel, J. M., and Wahl, G. M., 2004. Accelerated MDM2 auto-degradation induced by DNA-damage kinases is required for p53 activation. EMBO J, 23, pp. 1547-1556.

Stommel, J. M., and Wahl, G. M., 2005. A new twist in the feedback loop: stress-activated MDM2 destabilization is required for p53 activation. Cell Cycle 4 (3), pp. 411-417.

Thomas, R., 1973. Boolean formalization of genetic control circuits. J. Theor. Biol. 42, pp. 563-585.

Thomas, R., 1978. Logical Analysis of Systems Comprising Feedback Loops. J. Theor. Biol. 73, pp. 631-656.

Thomas, R., 1979. Some biological examples. Lecture Notes in Biomathematics 29, pp. 354-401.

Thomas, R., 1991. Regulatory networks seen as asynchronous automata: A logical description. J. Theor. Biol.153, pp. 1-23.

Thomas, R. and D'Ari, R., 1990. Biological Feedback. C.R.C. Press, Boca Raton, Florida, 316 pp.

Thomas, R. and Kaufman, M., 2001a. Multistationarity, the basis of cell differentiation and memory II. Logical analysis of regulatory networks in terms of feedback circuits. Chaos 11, pp. 180-195.

Thomas, R. and Kaufman, M., 2001b. Multistationarity, the basis of cell differentiation and memory I. Structural conditions of multistationarity and other nontrivial behavior. Chaos 11, pp. 170-179.

Thomas, R., Thieffry, D., Kaufman, M., 1995. Dynamical behaviour of biological regulatory networks-I. Biological role of feedback loops and practical use of the concept of the loop-characteristic state, Bulletin of Mathematical Biology 5(2), pp. 247-276.

Tiana, G., Jensen, M., and Sneppen, K., 2002. Time delay as a key to apoptosis induction in the p53 network. Eur. Phys. J. B. 29, pp. 135-140.

Vogelstein, B., Lane, D. and Levine, A. J., 2000. Surfing the p53 network. Nature 408 (6810), pp. 307-310.

Wagner, J., Ma, L., Rice, J. J., Hu, W., Levine, A. J., and Stolovitzky, G. A., 2005. p53-Mdm2 loop controlled by a balance of its feedback strength and effective dampening using ATM and delayed feedback. Syst. Biol. (Stevenage) 152 (3), pp. 109-118.

Weinberg, R. L., Veprintsev, D. B., and Fersht, A. R., 2004. Cooperative binding of tetrameric p53 to DNA. J. Mol. Biol. 341 (3), pp. 1145-1159.

Xirodimas, D. P., Saville, M. K., Bourdon, J.-C., Hay, R. T., and Lane, D. P., 2004. Mdm2-mediated NEDD8 conjugation of p53 inhibits its transcriptional activity. Cell 118 (1), pp. 83-97.

Zhang, T., Brazhnik, P., and Tyson, J. J., 2007. Exploring mechanisms of the DNA-damage response: p53 pulses and their possible relevance to apoptosis. Cell Cycle 6 (1), pp. 85-94.

Table legends

Table 1: Bifurcation conditions for the transition graph in Figure 5(a). For each bifurcation, the complementary inequalities determine the conditions for the alternative branches of the bifurcations. $t_{\overline{P(1)}}$ and $t_{\overline{P(2)}}$ denote the off delays associated, respectively, with the transition 1 → 0 and 2 → 1 for P.

Table 2: Cycling conditions and cycling periods for the transition graph in Figure 5(a). $t^{b}_{\overline{Mn}}$ is the "basal" off delay associated with Mn in the absence of damage with $t^{b}_{\overline{Mn}} \geq t_{\overline{Mn}}$.

Table 3: Parameter values used for the simulation of the differential model (3).

Table B.1: State tables corresponding to the core network. (a) P acts on Mn above its first threshold (Figure 2(a)). (b) P acts on Mn above its second threshold (Figure 2(b)).

Figure captions

Figure 1: Schematic representation of the model. Normal arrows correspond to positive interactions, blunt arrows to negative interactions.

Figure 2: Graph of interactions of the core network. The vertices P, Mc and Mn correspond to p53, nuclear and cytoplasmic Mdm2, respectively. The labels of the edges indicate the sign of the interactions and the order of their threshold. Value 1 means that the corresponding threshold is the lowest one, and value 2 that it is the highest one. In Figure 2(a), we present the situation where P is active on Mn above its lowest threshold, and on Mc above its second threshold. Figure 2(b) shows the reverse case.

Figure 3: Logical bifurcation diagrams corresponding to the core network. Each column differs from the preceding one by the value of one logical parameter $K_{Mn,\{..\}}$ and each parameter set corresponds to a specific asymptotic behaviour (see text). In (a) and (b), P acts on Mn above its first threshold (Figure 2 (a)). In (c) and (d), P acts on Mn above its second threshold (Figure 2(b)). The logical state variables are ordered as follows: P, Mc and Mn. sss: stable steady state (indicated between brackets); uss: unstable steady state as defined in appendix A.2; lc: cyclic sequence of states or logical cycle. $K_{Mn,\{..\}}$=1,0 indicates that the column's limit set is valid for $K_{Mn,\{..\}}$= 1 and $K_{Mn,\{..\}}$=0.

Figure 4: Logical interaction graph including DNA damage. The labels on the edges indicate the sign of the interactions and corresponding threshold order.

Figure 5: Transition graphs describing all possible pathways starting from any initial state. For each set of parameter values, the dynamical potentialities of the network are derived through an asynchronous updating procedure. In these graphs, the nodes describe the states of the network and the edges represent the possible transitions between these states. The order of the variables in the state vectors is: P, Mc, Mn, and Dam. Stable steady states are indicated by open squares. The stable logical cycles in the presence and absence of damage are indicated in dark and light grey, respectively. The black arrows indicate the trajectories that can be followed after a damage inducing stress, starting from state (0011). In fig. 5(a) the values of the logical parameters governing the level of Mn correspond to the second column of the bifurcation diagram

3(a) when Dam = 0, and to the third column when Dam = 1. In fig. 5(b) they correspond to the first (for Dam = 0) and last (for Dam = 1) column of the bifurcation diagram 3(b). In fig. 5(c), the logical parameter values in the absence and presence of damage are, respectively, as in the first and second column of diagram 3(c). Finally, in fig. 5(d), they correspond to the second (for Dam = 0) and last (for Dam = 1) column of the bifurcation diagram 3(d).

Figure 6: Single cell response upon damage induction, for different initial damage levels and repair rates, in the case of the transition graph in Figure 5(a). Initially, the system is at the steady state [0010]. Damage is induced at time t = 10 and the system starts oscillating. With each p53 burst the delay associated with the disappearance of the damage ($t_{\overline{Dam}}$) is reduced until the condition to stop oscillating is fulfilled. After repair the system returns to steady state. Parameter values used: $t_{P1} = 2$, $t_{\overline{P1}} = 2$, $t_{P2} = 1$, $t_{\overline{P2}} = 1$, $t_{Mc} = 0.6$, $t_{\overline{Mc}} = 1$, $t_{Mn} = 0.3$, $t^{b}_{\overline{Mn}} = 1.5$. The ratio $t^{0}_{\overline{Mn}} / t^{0}_{\overline{Dam}}$ is chosen equal to 0.1. (a, b): initial damage delay $t^{0}_{\overline{Dam}} = 5$, repair efficiency $\tau = 1.5$. (c, d): higher initial damage delay $t^{0}_{\overline{Dam}} = 9$ but same repair efficiency $\tau = 1.5$. (e, f): higher initial damage delay $t^{0}_{\overline{Dam}} = 9$, and higher repair efficiency $\tau = 4$.

Figure 7: Sustained p53 oscillations despite damage repair, for a higher basal degradation rate of nuclear Mdm2. Parameter values are as in Fig. 6 (a, b) except for a lower basal off-delay $t^{b}_{\overline{Mn}} = 1$.

Figure 8: Cell population simulations. Each time course is the average of 100 stochastic simulations, each representing an individual cell. For each cell, $t^{0}_{\overline{Dam}}$, representing the initial damage level, is drawn at random from its distribution at the start of the simulation. (a) Starting from the rest state [0010], upon damage induction, all cells follow the same cyclic pathway 1B and return to steady state after repair. (b) Different cells may follow different cyclic pathways. Upon repair they can either return straight to the steady state or remain temporarily trapped on cycle 2 in a proportion of about 85/15. The dampening of the oscillations is more important than in (a) due to the fact that the different cycles (here, 1.B and 1.C) have different periods and amplitudes. The mean

values of the time delays are as in Fig. 6, except for $t^{0}_{Dam} = 10$, $\tau = 8$, $t^{b}_{Mn} = 2.1$ in (a) and $t^{b}_{Mn} = 1.2$ in (b).

Figure 9: Three bifurcation diagrams for the differential system (3) as a function of the degradation rate of nuclear Mdm2, d_{Mn}, and different values of K_{Mc}. Solid lines: stable steady states (sss). Dashed lines: unstable steady states (uss). Black and open circles correspond to the minima and maxima of stable (slc) and unstable (ulc) limit cycles, respectively. Parameter values are given in Table 3.

Figure 10: (a) Oscillation period and (b) mean value of p53, corresponding to the bifurcation diagram shown in Figure 9(c).

Figure 11: The temporal behaviour of the system depends on the efficiency of damage repair. Simulation of system (3) after induction of a high damage level, for $K_{Mc} = 5$ and two different repair rates k_{Dam}. (a): $k_{Dam} = 0.04\ h^{-1}$. (b): $k_{Dam} = 0.07\ h^{-1}$. Other parameter values are as in Table 3.

Figure A.1: Graphical illustration of the notion of strong and weak interactions in the Boolean framework.

Figure A.2: Graphical illustration of the functionality and characteristic state of a positive circuit.

Table1

	Bifurcation choice	Condition
a	2001 → 2101	$t_{\overline{Dam}} > t_{Mc}$
b	2101 → 2111	$t_{\overline{Dam}} > t_{Mc} + t_{Mn}$
c	2111 → 1111	$t_{\overline{Dam}} > t_{Mc} + t_{Mn} + t_{\overline{P(2)}}$
d	1111 → 0111	$t_{\overline{P(1)}} < t_{\overline{Mc}}$
e	1011 → 0011	$t_{\overline{P(1)}} < t_{\overline{Mc}} + t_{\overline{Mn}}$
f	1110 → 1010	$t_{\overline{P(1)}} > t_{\overline{Mc}}$
g	1010 → 1000	$t_{\overline{P(1)}} > t_{\overline{Mc}} + t^{b}_{\overline{Mn}}$

Table: 2

Cycle 1A	$C_{1A} = t_{\overline{Dam}} > t_{Mc} + t_{Mn} + t_{\overline{P(2)}}$ AND $t_{\overline{P(1)}} < t_{\overline{Mc}}$ $T_{1A} = t_{P(2)} + t_{Mc} + t_{Mn} + t_{\overline{P(2)}} + t_{\overline{Mc}} + t_{\overline{Mn}} + t_{P(1)}$
Cycle 1B	$C_{1B} = t_{\overline{Dam}} > t_{Mc} + t_{Mn} + t_{\overline{P(2)}}$ AND $t_{\overline{Mc}} < t_{\overline{P(1)}} < t_{\overline{Mc}} + t_{\overline{Mn}}$ $T_{1B} = T_{1A}$
Cycle 1C	$C_{1C} = t_{\overline{Dam}} > t_{Mc} + t_{Mn} + t_{\overline{P(2)}}$ AND $t_{\overline{Mc}} + t_{\overline{Mn}} < t_{\overline{P(1)}}$ $T_{1C} = t_{P(2)} + t_{Mc} + t_{Mn} + t_{\overline{P(2)}} + t_{\overline{Mc}} + t_{\overline{Mn}}$
Cycle 2	$C_2 = t_{\overline{P(1)}} > t_{\overline{Mc}} + t^{b}_{\overline{Mn}}$ $T_2 = t_{P(2)} + t_{Mc} + t_{Mn} + t_{\overline{P(2)}} + t_{\overline{Mc}} + t^{b}_{\overline{Mn}}$ with $t^{b}_{\overline{Mn}} > t_{\overline{Mn}}$

C = condition, T = period

Table:3

Rate constants (h^{-1})
$k_P = 25,\ k_{Mc} = 0.3, k'_{Mc} = 4,\ k_{Dam} = 0.05,$
$k_{in} = 0.45,\ k'_{in} = 0.4, k_{out} = 0.045,$
$d_P = 0.02,\ d'_P = 0.3,\ d_{Mc} = 0.5,\ d'_{Mn} = 0.5,\ d''_{Mn} = 1.4$
Other parameters (dimensionless)
$K_{Dam} = 0.005,\ K_{Mn} = 20,\ V_r = 10.$

Table:B1

(a)

P	Mc	Mn	P	Mc	Mn
0	0	0	K_P	K_{Mc}	K_{Mn}
1	0	0	K_P	K_{Mc}	$K_{Mn,\{P\}}$
2	0	0	K_P	$K_{Mc,\{P\}}$	$K_{Mn,\{P\}}$
0	1	0	K_P	K_{Mc}	$K_{Mn,\{Mc\}}$
1	1	0	K_P	K_{Mc}	$K_{Mn,\{P,Mc\}}$
2	1	0	K_P	$K_{Mc,\{P\}}$	$K_{Mn,\{P,Mc\}}$
0	0	1	$K_{P,\{Mn\}}$	K_{Mc}	K_{Mn}
1	0	1	$K_{P,\{Mn\}}$	K_{Mc}	$K_{Mn,\{P\}}$
2	0	1	$K_{P,\{Mn\}}$	$K_{Mc,\{P\}}$	$K_{Mn,\{P\}}$
0	1	1	$K_{P,\{Mn\}}$	K_{Mc}	$K_{Mn,\{Mc\}}$
1	1	1	$K_{P,\{Mn\}}$	K_{Mc}	$K_{Mn,\{P,Mc\}}$
2	1	1	$K_{P,\{Mn\}}$	$K_{Mc,\{P\}}$	$K_{Mn,\{P,Mc\}}$

(b)

P	Mc	Mn	P	Mc	Mn
0	0	0	K_P	K_{Mc}	K_{Mn}
1	0	0	K_P	$K_{Mc,\{P\}}$	K_{Mn}
2	0	0	K_P	$K_{Mc,\{P\}}$	$K_{Mn,\{P\}}$
0	1	0	K_P	K_{Mc}	$K_{Mn,\{Mc\}}$
1	1	0	K_P	$K_{Mc,\{P\}}$	$K_{Mn,\{Mc\}}$
2	1	0	K_P	$K_{Mc,\{P\}}$	$K_{Mn,\{P,Mc\}}$
0	0	1	$K_{P,\{Mn\}}$	K_{Mc}	K_{Mn}
1	0	1	$K_{P,\{Mn\}}$	$K_{Mc,\{P\}}$	K_{Mn}
2	0	1	$K_{P,\{Mn\}}$	$K_{Mc,\{P\}}$	$K_{Mn,\{P\}}$
0	1	1	$K_{P,\{Mn\}}$	K_{Mc}	$K_{Mn,\{Mc\}}$
1	1	1	$K_{P,\{Mn\}}$	$K_{Mc,\{P\}}$	$K_{Mn,\{Mc\}}$
2	1	1	$K_{P,\{Mn\}}$	$K_{Mc,\{P\}}$	$K_{Mn,\{P,Mc\}}$

Fig:1

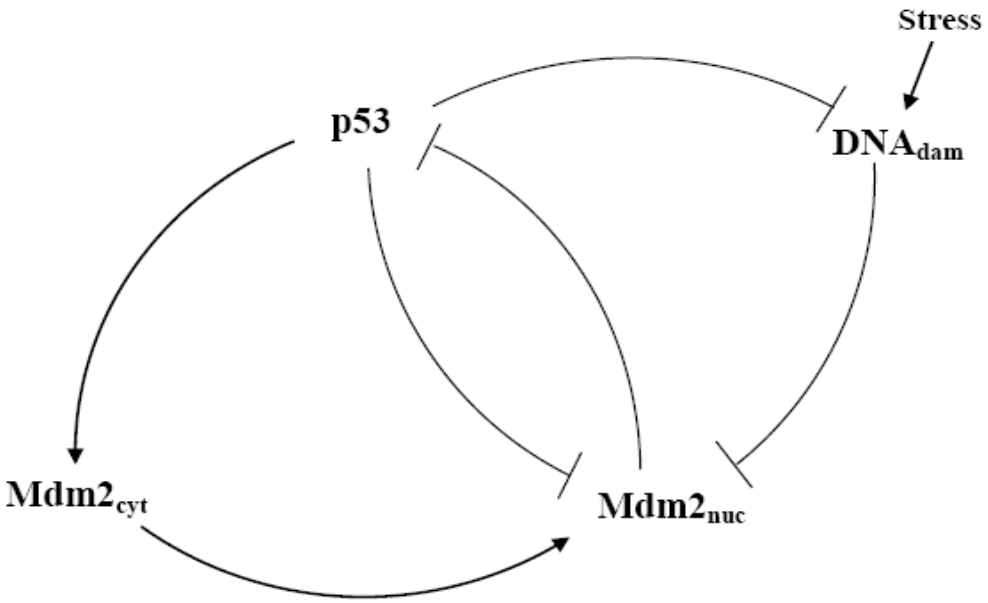

Fig:2

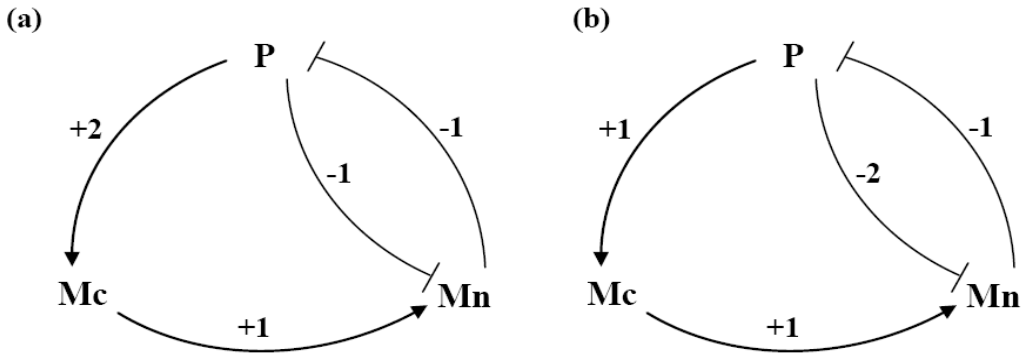

Fig:3

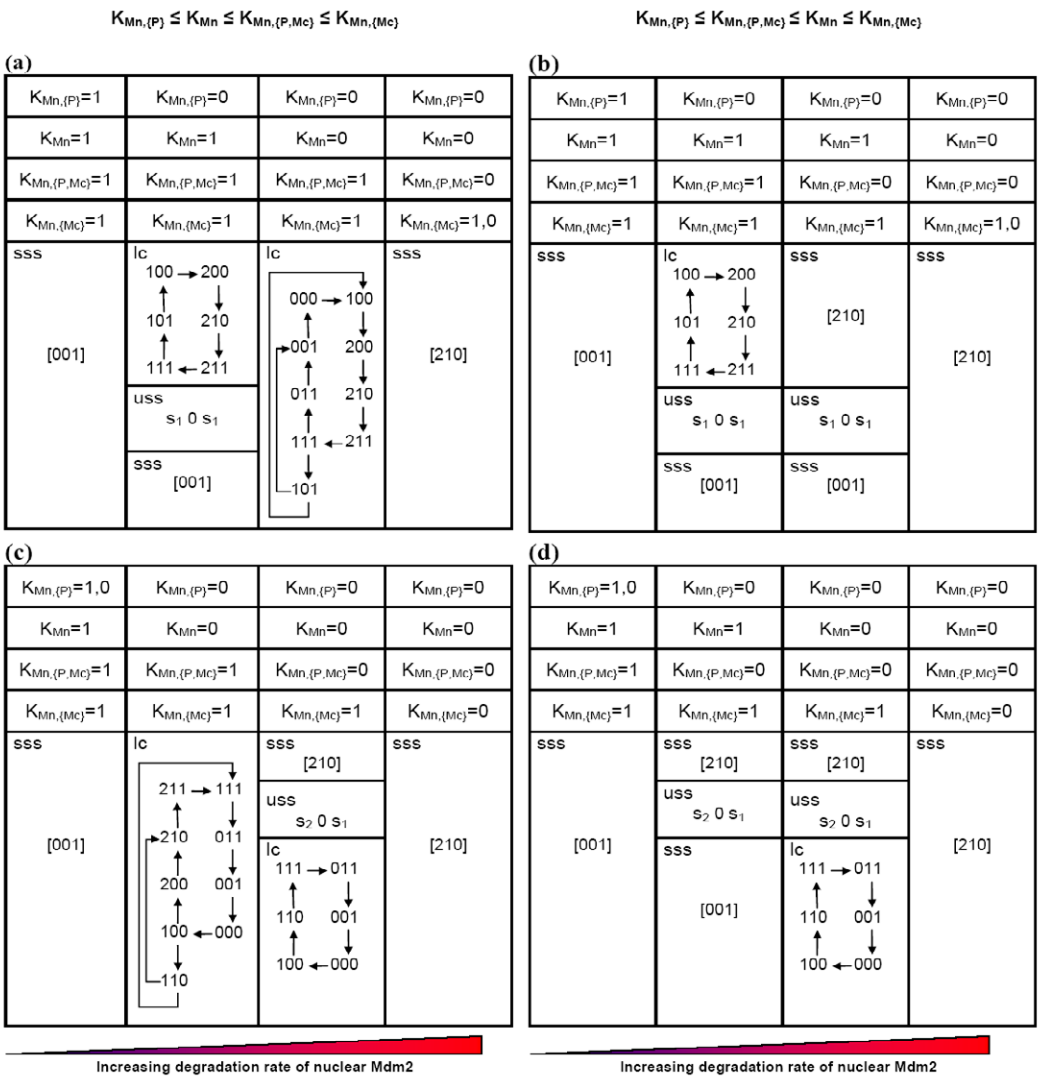

Fig:4

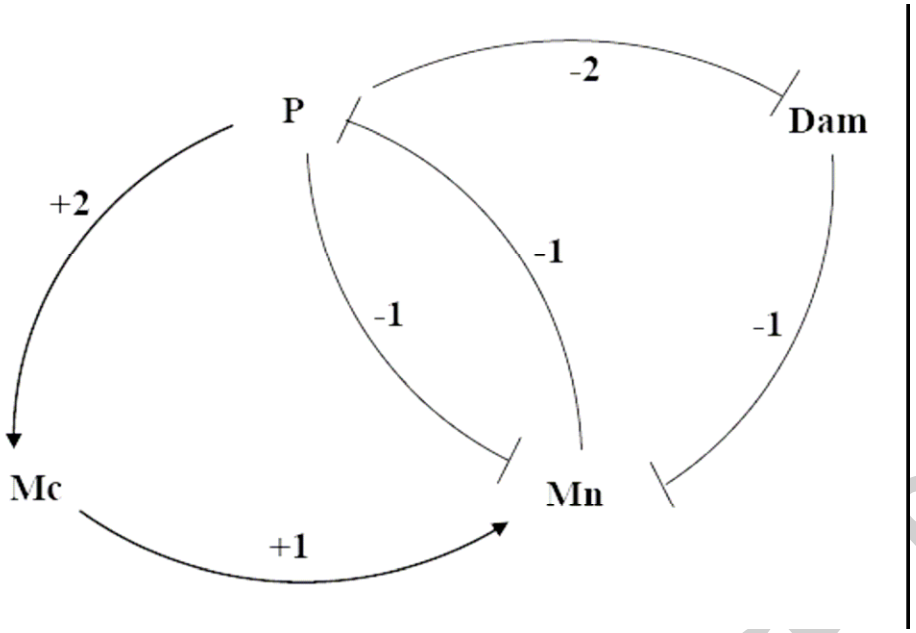

Fig:5

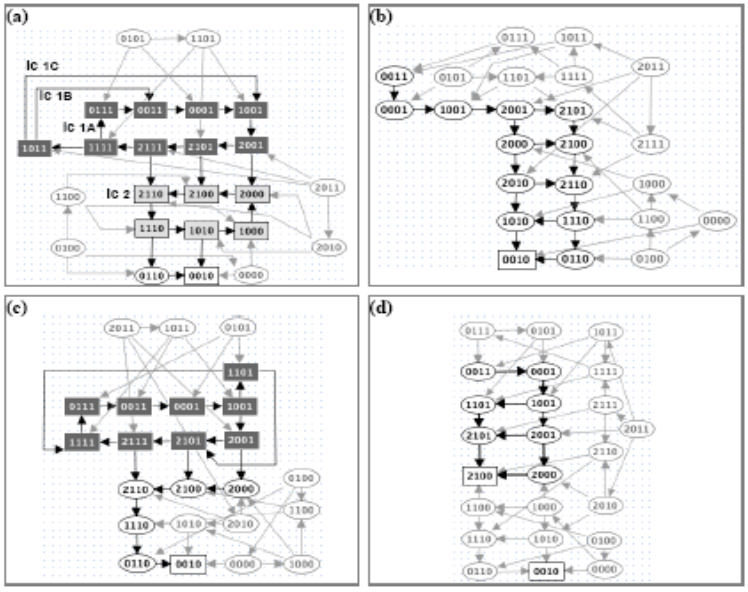

Fig:6

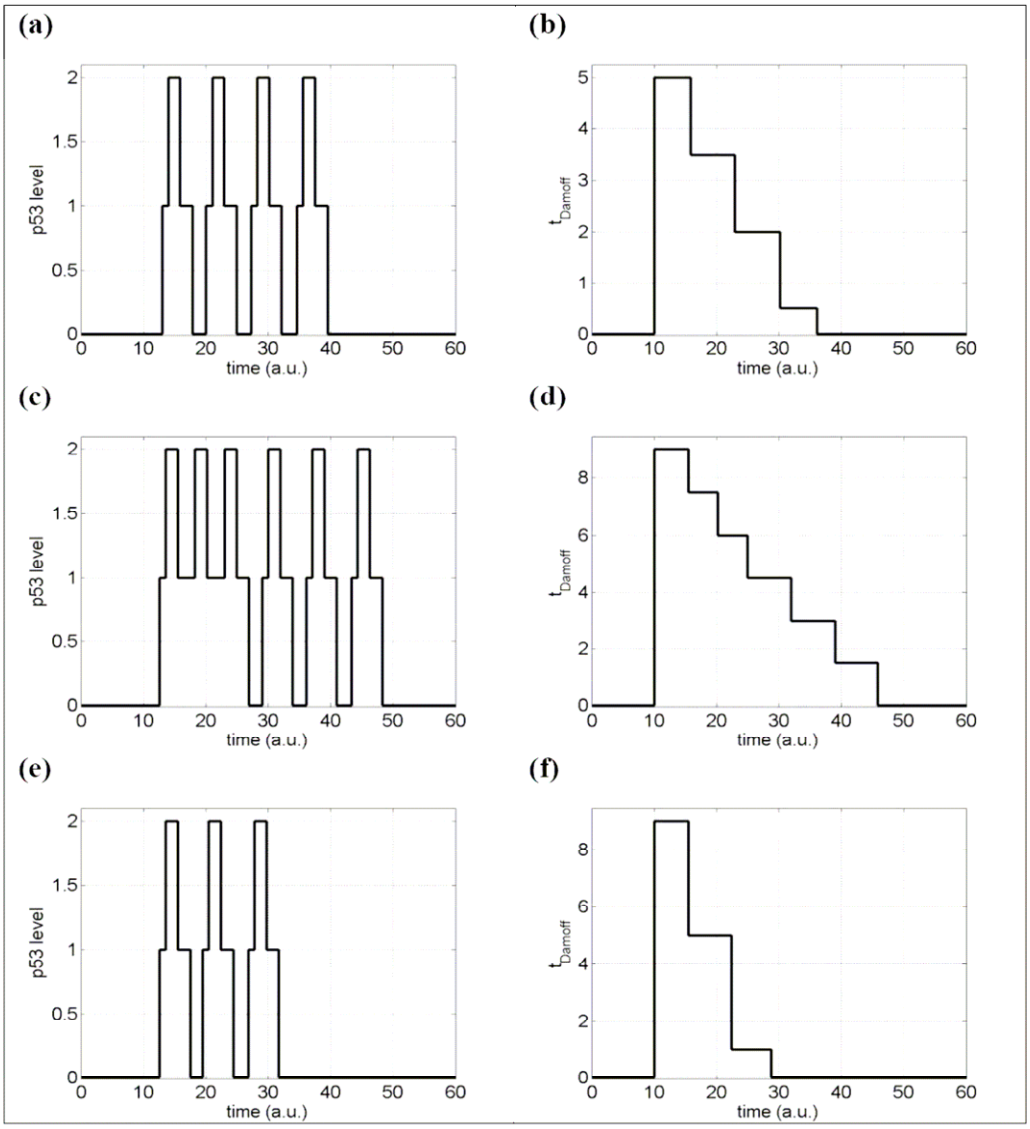

Fig:7

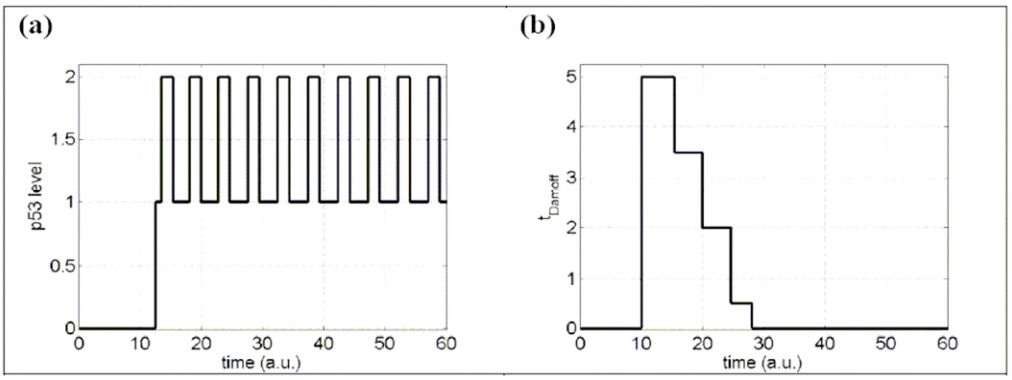

Fig:8

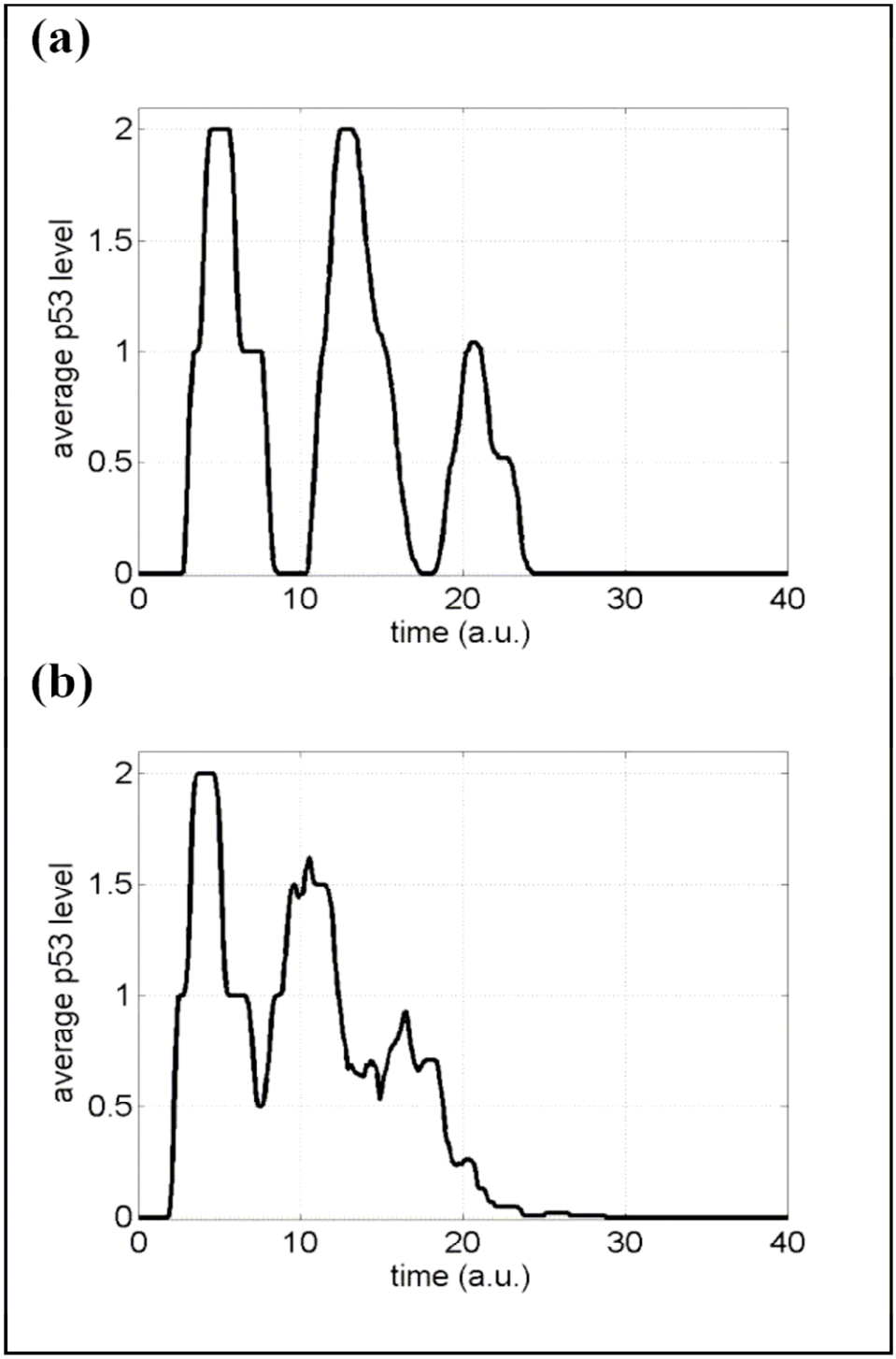

Fig:9

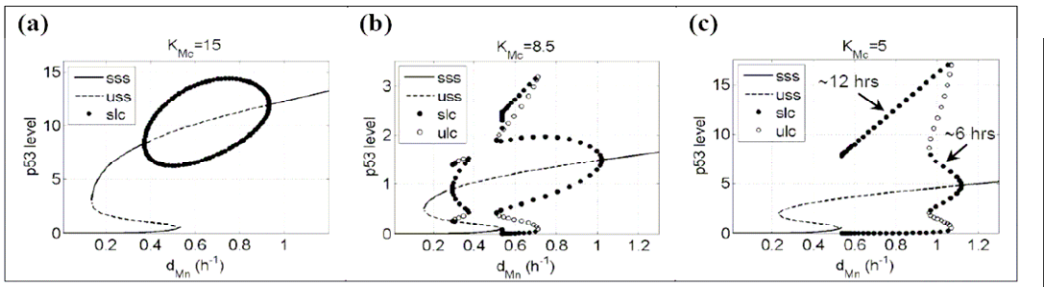

Fig:10

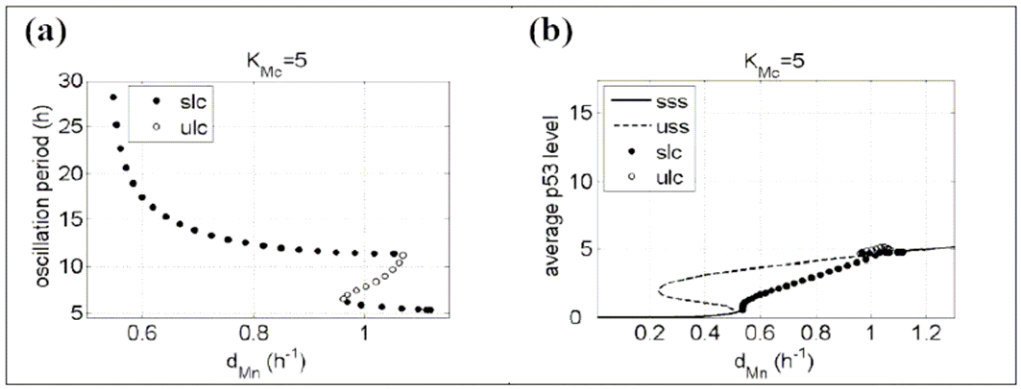

Fig:11

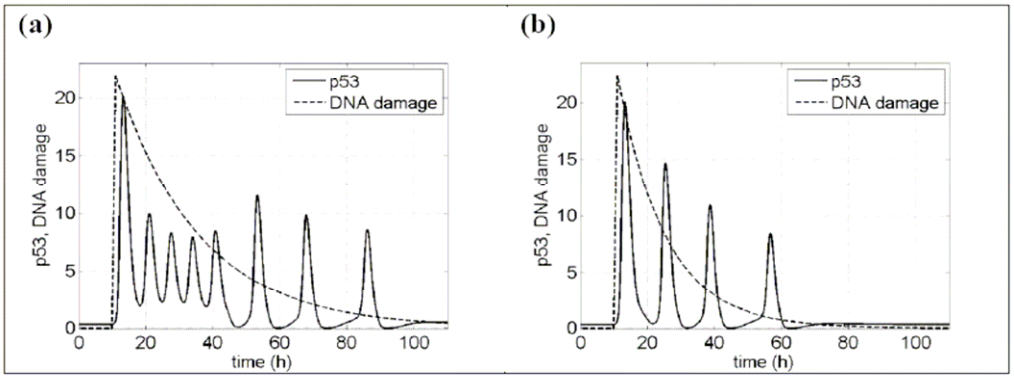

Fig:A1

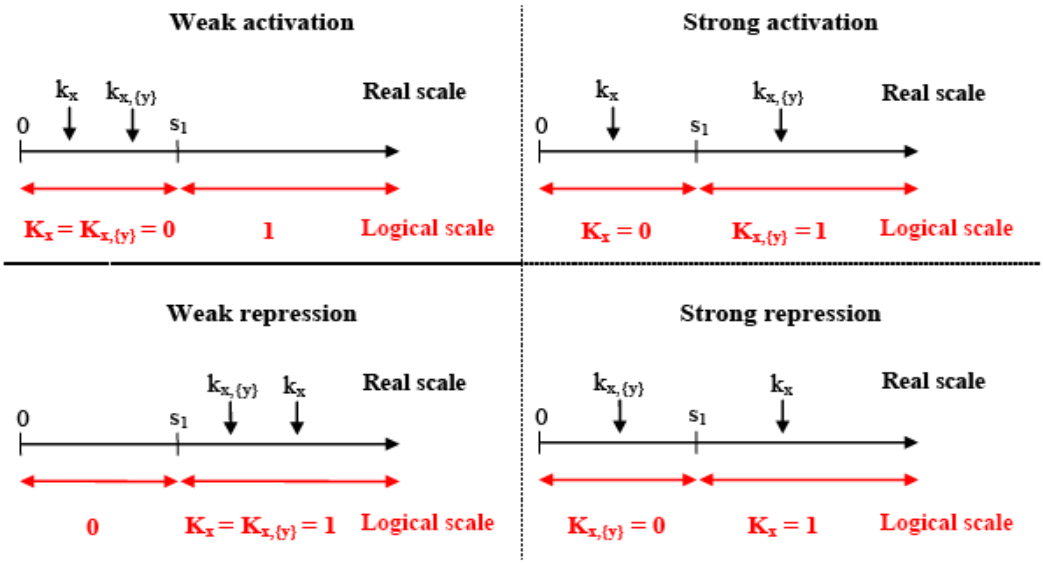

Fig:A2